diameter epoxy molds and polished to expose the greatest number of melt inclusions. Reflected light images of melt inclusions were used to document inclusion sizes and confirm that rehomogenization resulted in the melting of all daughter crystals.

Analytical techniques

Olivine grains, trapped spinel inclusions, and melt inclusions were analyzed by electron microprobe (Cameca SX-50 and SX-100) at Oregon State University for major- and volatile (S,Cl) elements. Beam sizes varied from 4-10 μm depending on inclusion size. Olivine grains and spinel inclusions were analyzed with a focused 1 μm electron beam. Constant beam conditions, with a 15 KeV accelerating voltage and 30 nA and 50 nA beam current, for glass and mineral phases, respectively, were utilized throughout the analytical sessions. The glass analytical procedure was optimized for analysis of S (30 sec peak count time) and Cl (100 sec peak count time). Repeat analyses of BCR-2G and LO-02-04ii glasses were made as external standards and Makaopuhi Lava Lake glass (USNM 113498/1 VG-A99), chromite (USNM 117075), and Springwater meteorite olivine (USNM 2566) were analyzed as internal standards under identical analytical conditions.

Following analysis, melt inclusion compositions are recalculated to be in equilibrium with their host olivine by adding olivine to the melt composition until an olivine-melt K_D^{Fe-Mg} of 0.3 is obtained (Roedder and Emslie, 1970; Sobolev and Chaussidon, 1996). Fe^{3+}/Fe^{2+} ratios required for recalculations were determined following the method of Danyushevsky (2000). For the forearc shoshonitic basalt, melt Fe^{3+}/Fe^{2+} ratios were calculated with the empirical calibration of Sack et al (1980) using

calculated fO_2 from sulfur peak shift measurements. A detailed description of this method is described in Chapter 2. Only rehomogenized inclusions with sulfur concentrations at or above the Fe-sulfide saturation curve (Wallace and Carmichael, 1992) are considered in this study. Sulfur concentrations below the Fe-sulfide saturation curve often occur in breached inclusions that have the greatest potential for contamination during rehomogenization and therefore likely do not maintain the composition of the original trapped melt (Nielsen et al., 1998). Low Cl concentrations coinciding with S concentrations below the Fe-sulfide saturation curve provide secondary evidence for degassing. In addition, inclusion compositions are carefully monitored for evidence of post-entrapment re-equilibration or Fe-loss (Danyushevsky et al., 2000, 2002).

Trace element concentrations in melt inclusions were determined by laser ablation (LA) ICP-MS analysis using a NewWave DUV 193 nm ArF Excimer laser and VG PQ ExCell Quadrupole ICP-MS at Oregon State University. Detailed analytical conditions and standard reproducibility are reported by Kent et al (2004) and Rowe et al (2006). Melt inclusions were ablated with a 30-50 µm laser spot, depending on inclusion diameter. Trace element abundances were calculated relative to the USGS glass standard BCR-2G, with ^{43}Ca as the normalizing isotope. For monitoring of accuracy and precision of melt inclusion analysis, USGS glasses BCR-2G and BHVO-2G were repeatedly analyzed over the course of each analytical session. Based on repeat analysis of BHVO-2G, trace element analyses by LA-ICP-MS are generally accurate to within 10% of accepted values (Appendix Table A9).

Sulfur speciation in melt inclusions was determined based on the relative shift of the S Kα peak position as determined by electron microprobe analysis after Carroll and Rutherford (1988) and Wallace and Carmichael (1994). Sulfur speciation measurements were made on a Cameca SX-50 at University of Oregon (UO) and a Cameca SX-100 at Oregon State University (OSU). Wave scans of the S Kα peak were simultaneously made on three PET crystals for measurements at UO and on two PET and one LPET crystal for measurements at OSU. Each spectrometer was moved incrementally 0.00005 sin θ units for 100 steps with a 5 sec counting time for mineral standards (< 9 min total time) and 30 sec counting time for glasses (50 min total time). A gaussian curve was then fit to the wave scans to determine the sulfur peak position of the unknown and standards. Pyrrhotite ($Fe_{1-x}S$; UO) and troilite (FeS; OSU) were analyzed before and after each unknown glass. Analysis of troilite at UO relative to the pyrrhotite standard does not indicate a significant shift between the two reduced sulfur standards allowing for a direct comparison between measurements made at UO and OSU. Additionally, pyrite (FeS_2) and anhydrite ($CaSO_4$) mineral grains were analyzed at the beginning and end of each analytical session.

To avoid oxidation of the sulfur during the glass analysis, occurring when beam exposure time is greater than ~10 minutes, the microprobe stage is moved 1 μm/min during continuous wave scan analysis (Rowe et al., in prep; Wallace and Carmichael, 1994). As a result of incrementally stage movement, melt inclusions with a diameter of less than 30 μm are not suitable for analysis with this technique. Due to the short time of analysis of reference minerals a stationary stage is acceptable (Rowe et al., in prep).

To determine reproducibility of sulfur speciation measurements we ran 6 repeat analyses of Galapagos Spreading Center (95.5°W) glass K 14-3 (Christie et al., 1986). The standard deviation (1σ) of the six repeat analyses was $\pm$ 3.5% sulfate. Propagation of error (1σ) associated with the peak fit of a single spectrometer wave scan, and the standard deviation (1σ) of the three spectrometer measurements per analysis, are roughly equivalent to the error estimated by repeat analysis of K 14-3 glass. The peak fitting error is largely dependant on sulfur concentration of the melt inclusion and increases with decreasing sulfur content.

Whole rock $^{40}Ar/^{39}Ar$ age determination of the forearc shoshonitic basalt (QV03-1) was conducted at Oregon State University following the procedure described in Duncan and Keller (2004) and Duncan et al (1997). Results are summarized in Appendix E.

ACROSS ARC COMPOSITIONAL VARIABILITY

Major- and trace-elements

Geochemical comparisons between forearc, arc and backarc basalts are subdivided based on classification as either shoshonitic, OIB-like, CAB, or LKT to reduce compositional variability potentially resulting from multiple mantle sources (see later discussion; Leeman et al., 2005; Conrey et al., 1997). However, in doing this, we make the assumption that the source for each basalt group, barring modification from the addition of a subduction component, is essentially the same across the arc. This assumption is supported by similarities between more fluid-immobile element (HFSE,

Table 9: Representative melt inclusion compositions.

Sample[1]	LL02-2		DB04-1			CC02-1	
Inclusion #	03-047-23.1	04-018-2.1	04-054-5/6	04-054-5/1	04-054-5/12	03-008-19.1	03-041-8.1
Corrected Melt inclusions (wt%)[2]							
SiO_2	45.72	50.04	49.45	50.13	51.16	49.09	50.19
TiO_2	1.60	1.45	1.40	1.41	1.41	1.07	1.00
Al_2O_3	15.64	17.60	16.15	17.62	18.49	17.64	18.09
Fe_2O_3	1.81	1.64	1.85	2.08	1.91	1.39	1.68
FeO	9.78	6.96	9.56	8.13	6.89	7.59	7.22
MnO	0.07	0.11	0.18	0.15	0.14	0.13	0.15
CaO	10.12	9.90	8.78	9.67	9.53	9.65	9.86
MgO	11.14	7.30	9.46	7.39	6.25	9.51	7.54
K_2O	0.64	0.87	0.54	0.50	0.58	0.57	0.66
Na_2O	3.10	3.63	2.29	2.56	3.26	3.15	3.27
P_2O_5	0.35	0.40	0.26	0.30	0.32	0.20	0.22
S	0.13	0.11	0.07	0.10	0.10	0.09	0.11
Cl	0.06	0.06	0.03	0.04	0.03	0.06	0.06
Total	100.19	100.12	100.05	100.11	100.08	100.14	100.09
S^{6+}/S_{tot} (%)[4]							3.7
Fe^{3+}/Fe_{tot}	0.14	0.17	0.15	0.19	0.20	0.14	0.17
Wt% Ol[3]	8.4	-2.4	11.8	2.5	-1.7	3.1	-1.4
Host Fo#	87.1	86.5	85.5	84.4	84.3	88.0	86.1
LA-ICP-MS Trace elements							
Sc	25.4			27.4	28.3		29.4
Ti	11560			8277	7655		6170
V	291.3						
Rb	11.3			8.5	7.5		11.2
Sr	798			454	413		452
Y	26.8			25.0	24.0		19.5
Zr	162			124	122		91
Nb	17.6			8.1	7.4		7.3
Ba	433			212	202		206
La	19.3			10.5	9.8		8.0
Ce	51.1			27.1	27.1		23.9
Pr	6.6			3.6	3.5		2.8
Nd	26.8			15.7	15.7		12.3
Sm	6.9			4.2	3.7		3.1
Eu	1.6			1.3	1.6		0.9
Gd	6.7			4.4	4.4		2.5
Dy	4.3			4.5	4.5		2.8
Er	2.9			2.4	2.3		1.6
Yb	1.9			2.4	2.4		1.8
Hf	4.1						
Ta	1.1			0.4	0.4		
Pb	6.4			3.2	2.8		2.8
Th	2.4			0.8	0.7		1.2
U				0.3	0.3		0.5

Notes: [1]Sample prefixes correspond to whole rock sample numbers in Table 1. [2]Melt inclusion compositions are recalculated to be in equilibrium with their host olivine (see text). [3]Wt% Ol (olivine) is the amount of olivine that must be either added or subtracted from the melt composition for the melt and olivine to be in equilbrium (assuming a olivine-melt K_D^{Fe-Mg} of 0.3; Roedder and Emslie, 1970). [4]Negative S^{6+}/S_{total} values are within error of 0.

Table 9: Continued

Sample	BC02-1		BR02-2		BB03-1		KWB03-1	
Inclusion #	03-016-9.1	03-016-59.1	03-049-3.1	03-071-9.1	03-065-2.1	03-065-16.2	03-067-13.1	03-067-11.1
Corrected Melt inclusions (wt%)								
SiO_2	47.80	49.57	49.17	50.32	48.87	52.14	51.72	54.45
TiO_2	1.32	1.73	1.35	1.21	1.45	1.66	1.51	1.67
Al_2O_3	16.68	17.63	16.80	17.21	16.48	17.23	16.00	17.55
Fe_2O_3	2.26	3.57	1.43	2.44	2.76	3.52	2.67	3.00
FeO	9.63	8.61	7.78	7.91	9.67	6.56	8.06	5.83
MnO	0.09	0.18	0.10	0.25	0.18	0.18	0.18	0.14
CaO	8.79	6.82	9.76	9.73	8.29	9.08	8.13	7.29
MgO	9.35	6.37	9.92	6.86	8.27	4.53	6.65	4.14
K_2O	0.53	0.47	0.48	0.59	0.62	1.03	0.87	1.11
Na_2O	3.24	4.63	2.96	3.16	2.98	3.80	3.72	4.37
P_2O_5	0.28	0.38	0.21	0.24	0.42	0.26	0.43	0.45
S	0.09	0.13	0.08	0.08	0.12	0.11	0.12	0.11
Cl	0.02	0.03	0.03	0.05	0.04	0.04	0.06	0.06
Total	100.10	100.17	100.10	100.12	100.15	100.16	100.15	100.18
S^{6+}/S_{tot}								
Fe^{3+}/Fe_{tot}	0.17	0.27	0.14	0.22	0.20	0.33	0.23	0.32
Wt% Ol^3	3.1	-5.0	1.9	-4.2	1.3	-8.6	-3.8	-8.7
Host Fo#	85.2	81.5	88.3	83.7	83.6	80.4	83.1	80.8
LA-ICP-MS Trace elements								
Sc	35.7	24.7	27.6	26.5		28.6		22.8
Ti	8038	9854	8632	8301		9717		8573
V	220.9	258.1	241.2					
Rb	11.2	6.0	11.2	10.5		26.5		17.3
Sr	491	554	419	356		405		446
Y	26.2	37.6	20.4	17.3		26.5		24.7
Zr	135	193	96	75		118		113
Nb	9.9	9.6	9.3	7.8		7.4		7.7
Ba	244	177	248	197		382		358
La	11.8	11.9	9.9	7.8		11.4		11.7
Ce	33.4	29.1	24.9	21.5		31.3		29.4
Pr	3.1	4.2	3.6	2.7		3.9		4.1
Nd	16.7	20.1	14.4	11.6		16.7		17.6
Sm	4.5	4.5	2.6	2.9		4.2		4.4
Eu	2.0	2.3	1.4	1.1		1.5		1.4
Gd		7.0	4.4	3.3		4.6		4.8
Dy	3.4	6.7	3.8	2.9		4.6		4.4
Er	3.0	3.1	2.1	1.8		2.6		2.6
Yb	4.3	2.9	2.3	2.0		2.6		1.9
Hf	4.3	4.5	2.3	1.9		2.6		2.5
Ta	0.8	0.5		0.4		0.4		0.3
Pb	2.4	2.6	2.5	2.9		5.0		5.1
Th				0.9		2.0		1.4
U				0.5		0.9		0.6

Table 9: Continued

Sample	LTB02-2		AIC02-1		TB03-1		SIC02-1	
Inclusion #	03-074-17.1	03-074-8.1	03-073-6.1	03-073-11.1	04-028-7.1	03-076-12.1	03-011-68.1	03-011-12.1
Corrected Melt inclusions (wt%)								
SiO_2	48.29	50.35	48.74	50.39	47.31	52.53	49.01	50.87
TiO_2	1.26	1.35	1.38	1.38	2.36	1.14	1.29	1.33
Al_2O_3	17.72	19.41	18.64	19.83	17.71	19.73	17.50	16.06
Fe_2O_3	2.09	1.77	1.70	1.50	1.47	1.16	2.84	4.28
FeO	8.35	6.25	7.03	5.62	7.23	5.05	8.82	8.52
MnO	0.17	0.09	0.13	0.12	0.10	0.12	0.19	0.24
CaO	9.70	10.22	10.82	10.99	10.51	9.65	9.51	9.25
MgO	7.94	5.92	7.24	5.69	8.76	5.77	7.30	5.83
K_2O	0.62	0.64	0.56	0.58	0.56	0.78	0.36	0.36
Na_2O	3.43	3.59	3.33	3.57	2.52	3.82	2.96	3.01
P_2O_5	0.41	0.34	0.38	0.30	1.43	0.17	0.20	0.20
S	0.10	0.11	0.08	0.10	0.11	0.08	0.11	0.11
Cl	0.03	0.04	0.02	0.03	0.03	0.05	0.03	0.03
Total	100.13	100.13	100.09	100.12	100.11	100.11	100.13	100.12
S^{6+}/S_{tot}					1.60			
Fe^{3+}/Fe_{tot}	0.18	0.20	0.18	0.19	0.15	0.17	0.22	0.31
Wt% Ol[3]	0.4	-5.4	-2.7	-6.3	-1.6	-4.5	-2.8	-5.0
Host Fo#	85.0	84.9	85.9	85.7	87.8	87.2	78.5	80.1
LA-ICP-MS Trace elements								
Sc		33.0		25.6	31.8	19.1	31.6	25.4
Ti		7461		8522	12688	6195	7808	6576
V								
Rb		5.5		7.9	10.3	11.4	5.9	5.3
Sr		454		418	308	525	339	316
Y		19.8		22.1	22.6	15.9	20.9	16.5
Zr		94		107	117	86	67	62
Nb		7.7		8.7	10.2	6.0	5.2	4.4
Ba		248		186	182	295	130	123
La		9.2		8.6	10.4	8.8	5.0	4.8
Ce		24.4		22.1	27.8	22.6	17.2	14.6
Pr		2.9		3.0	3.9	2.9	2.2	2.0
Nd		13.1		13.0	17.1	12.3	10.1	8.9
Sm		3.4		3.5	3.2	2.7	2.5	2.1
Eu		1.1		1.1	0.9	1.0	1.1	1.1
Gd		4.4		3.4	3.7	2.7	3.5	2.5
Dy		3.5		3.6	3.1	2.8	3.0	2.7
Er		2.1		1.8	2.4	1.7	2.3	1.5
Yb		2.0		1.7	2.1	1.3	2.4	1.7
Hf		2.1		2.1		1.9	1.4	1.3
Ta		0.5		0.6	0.5	0.4	0.2	0.3
Pb		2.5		2.1	3.0	3.6	1.9	1.3
Th		0.8		0.6	1.2	0.8	0.5	0.6
U		0.3		0.3	0.6	0.3	0.2	0.2

Table 9: Continued

Sample	ELK02-1		FLR03-1		BYC02-1		NEF03-1	
Inclusion #	02-023-4-B-1	02-022-3-A-2	03-040-22.1	05-017-12	04-027-12.1	04-027-3.1	05-013-3/14	05-013-3/22
Corrected Melt inclusions (wt%)								
SiO_2	47.79	50.24	44.73	49.63	46.14	47.53	48.10	49.42
TiO_2	1.48	1.47	1.83	1.77	2.00	2.10	2.02	2.06
Al_2O_3	14.98	17.31	17.13	18.71	16.18	17.26	17.05	18.17
Fe_2O_3	4.27	2.99	2.61	2.04	6.02	6.12	3.00	2.80
FeO	10.18	7.78	10.05	7.07	10.33	7.43	8.40	6.90
MnO	0.21	0.15	0.15	0.18	0.25	0.20	0.18	0.19
CaO	9.02	9.19	11.15	10.35	9.30	9.86	10.41	10.55
MgO	7.15	5.87	9.85	6.50	6.66	4.48	6.65	5.32
K_2O	0.69	0.87	0.33	0.52	0.52	0.56	0.47	0.57
Na_2O	3.80	3.59	1.89	2.78	2.24	4.03	3.32	3.61
P_2O_5	0.40	0.54	0.26	0.35	0.32	0.38	0.38	0.37
S	0.13	0.10	0.12	0.11	0.11	0.16	0.21	0.14
Cl	0.04	0.04	0.02	0.04	0.02	0.03	0.03	0.03
Total	100.18	100.14	100.14	100.08	100.13	100.17	100.22	100.15
S^{6+}/S_{tot}				7.40			14	-0.5
Fe^{3+}/Fe_{tot}	0.27	0.26	0.19	0.21	0.34	0.43	0.24	0.27
Wt% Ol^3	1.0	-2.7	-5.0	-4.9	-3.9	-7.6	-4.1	-7.3
Host Fo#	80.7	81.8	85.3	84.5	79.3	78.2	82.5	82.1
LA-ICP-MS Trace elements								
Sc	36.9	95.4	25.7	24.8			39.6	29.6
Ti			10695	9565			10936	11206
V	188.7	134.3	258.7					
Rb	14.7	23.8	10.9	7.3			8.0	10.9
Sr	482	195	392	412			331	321
Y	34.8	20.8	31.9	25.8			30.4	31.2
Zr	166	103	138	121			132	142
Nb	10.0	6.3	10.0	9.0			10.9	12.3
Ba	754	152	389	242			147	171
La	12.6	7.2	8.8	9.4			9.5	10.8
Ce	30.8	16.8	23.8	26.7			28.7	27.9
Pr	4.0	2.4	3.4	3.6			3.6	3.8
Nd	19.4	8.1	18.2	16.2			16.6	17.7
Sm	4.9	3.1	4.4	4.2			4.1	3.6
Eu	2.0	1.3	1.7	1.5			1.6	
Gd	5.7	12.1	4.5	3.7			4.6	6.3
Dy	5.6	3.1	6.1	4.3			3.7	5.1
Er	3.4	1.8	3.0	2.4			2.8	3.3
Yb	3.3	1.4	3.2	2.4			2.1	3.1
Hf	4.1	3.4	1.4					
Ta				0.6			0.6	0.6
Pb	0.2	3.0	2.2	3.0			1.8	1.8
Th	1.4	0.8		0.7			0.9	1.0
U	0.4	0.5		0.4			0.5	0.3

Table 9: Continued

Sample	HL03-1		WF02-1			NMB03-1	
Inclusion #	03-045-7.1	03-044-6.1	03-014b-16.1	03-014b-1.1	05-011-1 / 4	04-024-5.1	04-026-8.1
Corrected Melt inclusions (wt%)							
SiO_2	42.82	48.41	48.19	48.53	49.21	43.72	49.30
TiO_2	2.50	2.24	1.74	1.86	1.82	2.82	1.77
Al_2O_3	16.93	17.75	18.19	18.26	19.62	16.22	18.13
Fe_2O_3	4.44	3.09	1.06	1.42	1.39	2.97	2.16
FeO	8.90	6.62	5.55	6.08	5.68	8.37	6.36
MnO	0.21	0.11	0.11	0.13	0.13	0.19	0.15
CaO	15.04	11.55	12.40	11.77	11.32	13.50	12.03
MgO	6.18	4.83	7.66	6.80	6.12	6.87	5.38
K_2O	0.41	0.81	0.63	0.53	0.56	0.07	0.67
Na_2O	2.26	4.16	3.90	4.04	3.60	3.05	3.64
P_2O_5	0.26	0.43	0.53	0.56	0.51	2.20	0.30
S	0.13	0.12	0.24	0.13	0.17	0.15	0.09
Cl	0.05	0.10	0.38	0.14	0.14	0.03	0.03
Total	100.18	100.23	100.62	100.28	100.29	100.17	100.06
S^{6+}/S_{tot}			22.1	5.3	11.3		
Fe^{3+}/Fe_{tot}	0.31	0.30	0.15	0.17	0.18	0.24	0.23
Wt% Ol[3]	-7.1	-8.3	-3.3	-5.2	-5.3	-8.1	-6.5
Host Fo#	82.8	82.6	88.6	86.5	86.5	83.0	83.4
LA-ICP-MS Trace elements							
Sc	31.3	23.3	28.6	28.4	33.3		
Ti	15389	12705	9787	10761	10030		
V	513.7	267.6					
Rb	6.5	12.2	4.5	4.0	3.8		
Sr	594	760	1755	927	838		
Y	34.3	27.4	24.3	28.6	27.6		
Zr	191	176	175	184	205		
Nb	15.1	22.1	13.0	12.8	10.8		
Ba	218	320	228	223	251		
La	16.9	18.3	23.0	17.2	15.5		
Ce	58.7	52.4	62.8	53.2	48.6		
Pr	6.3	6.3	7.7	6.2	6.0		
Nd	31.2	23.8	27.2	27.4	22.5		
Sm	6.8	6.0	4.9	5.4	4.9		
Eu	2.0	1.8	1.8	1.6	1.7		
Gd		4.3	4.8	5.8	4.2		
Dy	7.6	4.9	3.9	5.2	5.5		
Er	1.7	3.2	2.4	3.3	3.4		
Yb	2.8	1.7	2.0	2.0	2.7		
Hf	4.4	4.1					
Ta	1.3	1.4	0.8	0.8	0.5		
Pb	3.4	2.7	2.4	2.8	3.8		
Th	3.0	1.4	1.1	1.0	0.7		
U			0.5	0.3	0.3		

Table 9: Continued

Sample	BLW03-1		QV04-3b		CM02-2		
Inclusion #	03-048-61.1	03-072-7.1	04-050-20.1	04-050-17.1	03-002.-12.1	03-058-10.1	03-058-15.1
Corrected Melt inclusions (wt%)							
SiO_2	46.58	48.03	49.66	50.25	48.19	49.80	50.08
TiO_2	1.57	1.73	1.75	1.90	1.47	0.95	1.28
Al_2O_3	16.34	18.01	14.30	15.76	14.88	17.92	18.69
Fe_2O_3	1.69	2.14	2.20	2.27	1.81	1.08	1.04
FeO	8.73	7.70	5.64	4.84	8.12	5.11	4.96
MnO	0.16	0.15	0.13	0.12	0.15	0.08	0.08
CaO	10.51	10.79	9.47	10.15	11.54	12.18	11.51
MgO	10.04	7.12	8.16	5.04	8.86	6.32	6.23
K_2O	0.52	0.62	1.73	1.56	1.66	3.17	2.08
Na_2O	3.47	3.32	1.52	2.60	2.90	2.75	3.55
P_2O_5	0.36	0.36	1.23	1.38	0.38	0.63	0.47
S	0.11	0.11	0.43	0.44	0.12	0.50	0.38
Cl	0.02	0.04	0.15	0.15	0.11	0.12	0.07
Total	100.11	100.15	96.37	96.49	100.24	100.61	100.46
S^{6+}/S_{tot}		3.2	86.6	75.8		52.2	47
Fe^{3+}/Fe_{tot}	0.15	0.20	0.29	0.29	0.17	0.16	0.16
Wt% Ol^3	4.4	-3.3	6.8	-0.6	-2.0	-4.0	-4.3
Host Fo#	87.2	84.6	89.6	86.1	87.4	88.0	88.2
LA-ICP-MS Trace elements							
Sc	46.1	33.7	18.7	19.0	37.4	19.1	26.5
Ti	10292	9637	9367	11196	9014	5278	7294
V	231.9						
Rb	7.1	8.4	38.4	55.9	7.6	7.3	7.4
Sr	307	308	4055	4308	1434	3489	2065
Y	26.1	30.6	20.6	22.4	29.8	12.8	18.7
Zr	138	161	347	412	132	70	98
Nb	18.4	18.5	8.3	10.5	5.7	2.0	3.6
Ba	155	149	2428	4182	1645	1917	1079
La	13.3	13.0	92.2	106.5	33.8	42.6	24.5
Ce	31.3	31.5	241.9	323.4	99.8	134.1	84.8
Pr	3.6	4.1	31.3	37.6	13.7	17.8	10.4
Nd	13.0	18.7	122.9	138.2	59.9	74.3	40.6
Sm		4.5	19.0	22.3	11.7	10.4	5.8
Eu	1.4	1.5	4.7	6.0	3.6	3.2	2.1
Gd		5.0	10.3	11.5	6.0	5.2	4.7
Dy	3.9	5.3	4.7	6.2	5.8	2.7	3.5
Er		3.2	1.5	1.3	2.6	1.4	1.7
Yb		2.8	1.2	1.5	2.6	1.2	1.6
Hf	2.1				3.4		
Ta		1.1	0.3	0.7		0.1	0.2
Pb	2.5	1.6	20.6	28.8	15.9	18.7	11.7
Th		1.1	8.7	11.7	1.1	0.9	0.7
U		0.4	2.9	4.0		0.4	0.4

HREE) concentrations and ratios between melt inclusions within basalt groups from different regions across the volcanic arc. While trace element concentrations in melt inclusions are in some cases highly variable relative to whole-rock compositions, overall trends and ratios (i.e. Ce/Pb and K/Nb) are similar to those observed in the whole-rock samples (Table 8). This observation is significant in that it may suggest relatively limited interaction between basalt groups during melting or melt aggregation. Figure 20 illustrates the overall similarity between melt inclusions and whole rock trace element compositions for a representative example from each basalt group. Calc-alkaline basaltic melt inclusions tend to have the greatest variability relative to whole rock analyses, with compositions ranging from near LKT trace-element signatures to more typical CAB trace element signatures in some samples (Fig. 20). This variability however is sample dependent where some samples have very little variability in melt inclusion compositions (see Table 9 for representative compositions).

In general backarc OIB-like inclusion compositions are more mafic, with an average of 8.40 wt% MgO (10.91-5.38 wt% MgO) compared to an average of 6.40 wt% MgO (7.81-4.83 wt% MgO) for arc melt inclusions (Table 9, 10). Despite this distinction, K_2O concentrations between the arc and backarc are similar with an average of 0.54 wt% K_2O for arc basalts and 0.50 wt% K_2O for backarc basalts. Trace element concentrations are significantly different between the arc and backarc lavas. Arc OIB-like melt inclusions are enriched in light to middle rare earth elements (LREE-MREE) but have heavy rare earth elements equivalent to backarc OIB-like lavas. Despite a greater Nb and Ta depletion in arc OIB-like inclusions, Zr concentrations are somewhat

Figure 20. Representative primitive mantle normalized whole rock trace element compositions versus melt inclusions from the same sample. Representative basalt samples are; (A) Shoshonite forearc basalt QV04-3b (QV03-1), (B) Calc alkaline backarc basalt sample TB02-1, (C) LKT backarc basalt NEF03-1, and (D) OIB-like backarc basalt BLW03-1. Bold dashed line is the whole rock composition.
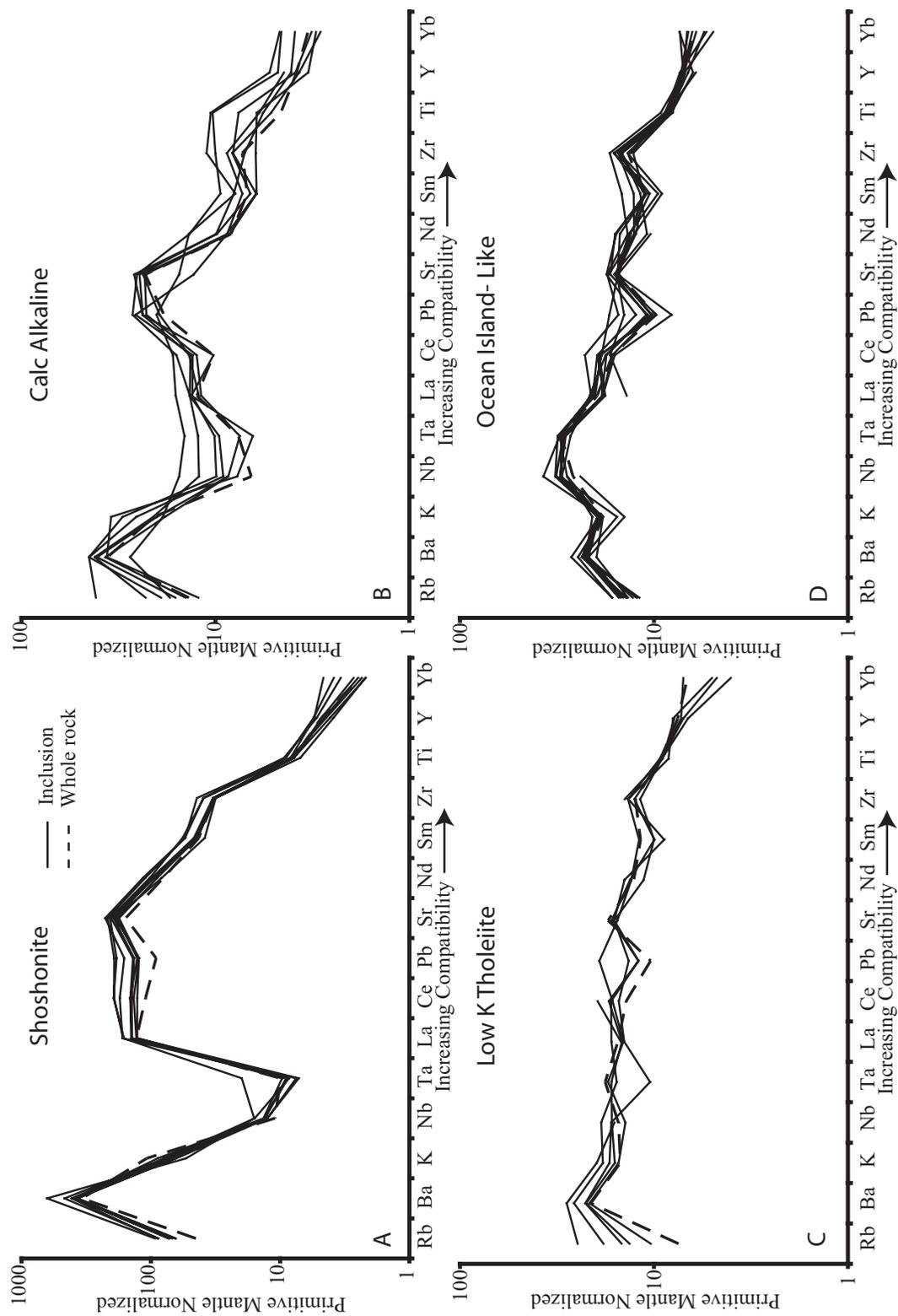
Figure 20.

greater relative to the backarc compositions (Fig. 21c). In addition, Ba, Pb, Sr and Ti concentrations are enriched in arc relative to backarc OIB-like inclusions.

Major and trace element compositions from low-K tholeiitic melt inclusions are very similar between melt inclusions from arc and backarc lavas. Arc LKT melt inclusions are on average more primitive with an average of 7.82 wt% MgO versus 5.96 wt% MgO for back arc inclusions. The only distinguishable difference between arc and backarc tholeiitic melt compositions is an enrichment in Ba, 233 to 389 ppm versus 142-186 ppm, and Sr, 341 to 435 ppm versus 290-330 ppm, in arc LKT's (Fig. 21d). REE and REE concentrations are identical between arc and backarc melt inclusions and are similar to OIB-like backarc concentrations, although on average lower in LREE concentrations.

Calc-alkaline basalts are the most abundant and compositionally variable basalt group in both the arc and backarc of the Oregon Cascades. Arc CAB melt inclusions are generally more primitive with an average of 8.09 wt% MgO (11.4-6.24 wt% MgO) compared to an average of 6.85 wt% MgO (10.51-3.21) for backarc CAB inclusions. K_2O concentrations between arc and backarc samples are equivalent with an average of 0.60 wt% (Table 9, 10). Despite the increased variability, as with the LKT melt inclusions, compositions from calc-alkaline basalts from the arc overlap with those of the backarc. In general backarc CAB's are more variable, and in some cases more enriched in fluid mobile elements, than comparable arc lavas (Fig. 21b). Strontium concentrations from arc CAB inclusions vary from 554-413 ppm, within the range but on average greater than concentrations in backarc CAB inclusions (532-259 ppm; Table 9, 10). In
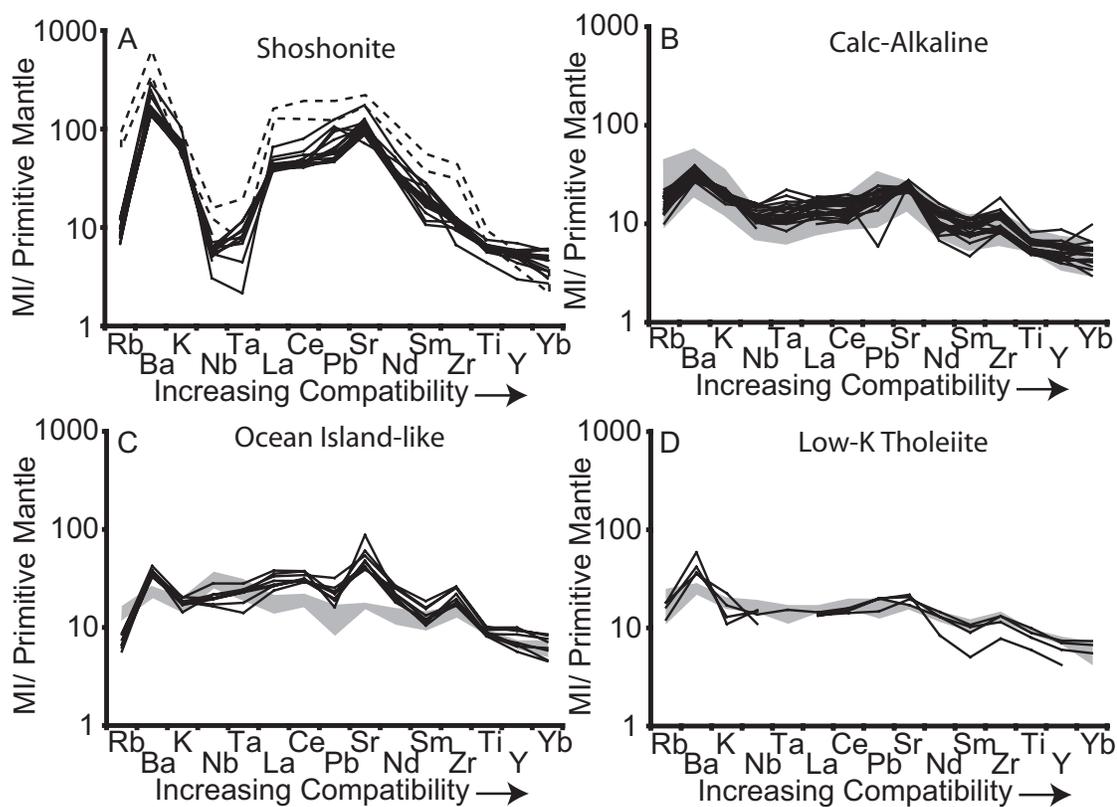
Figure 21. Primitive mantle normalized trace element diagrams for melt inclusions analyzed by laser ablation ICP-MS from (A) shoshonitic basalts, (B) calc-alkaline basalts, (C) ocean-island like basalts, and (D) low K tholeiitic basalts. Dashed field in (A) outlines the range of melt inclusion compositions from the forearc shoshonitic basalt. Shaded fields in (B-D) indicate range of basaltic compositions in backarc inclusions. Solid lines are individual analyses of melt inclusions from the arc.

Table 10: Range of selected major and trace elements from melt inclusions by location and basalt type[2].

| Location | FOREARC | | ARC | | | | | |
Type	SHOSH		SHOSH		CAB		LKT	
	Max	Min	Max	Min	Max	Min	Max	Min
MgO[1]	8.20	4.20	9.18	5.35	10.11	6.25	12.29	5.51
K$_2$O[1]	4.11	0.85	4.18	1.03	0.77	0.41	0.65	0.09
S[1]	0.58	0.09	0.50	0.07	0.13	0.01	0.16	0.06
Cl[1]	0.19	0.07	0.12	0.01	0.08	0.02	0.05	0.00
Sr	4504	3520	3489	1434	798	413	435	341
Y	23.7	16.6	29.8	12.8	37.6	17.1	31.9	18.0
Zr	461	330	132	70	193	84	138	82
Nb	10.5	8.2	5.7	2.0	17.6	6.0	10.0	7.2
Ba	4182	2428	1917	907	433	172	389	234
La	107.7	82.7	42.6	24.2	19.3	6.5	9.4	8.6
Ce	325.7	214.1	134.1	68.4	51.1	17.1	26.7	23.8
Yb	2.0	1.0	2.7	1.2	4.3	1.3	3.2	2.4
Pb	28.8	18.5	18.7	6.9	6.4	0.9	3.0	2.2
Th	11.7	8.7	1.2	0.5	2.4	0.6	1.7	0.7
U	5.3	2.7	0.5	0.2	0.6	0.3	0.4	0.4

Notes:[1] Major element and volatile compositions are recalculated to be in equilibrium with their host olivines (see text). [2]Compositions are not from single analyses but represent the overall range based on location and sample type.

Table 10: Continued

Location	ARC				BACKARC			
Type	OIB-like		CAB		LKT		OIB-like	
	Max	Min	Max	Min	Max	Min	Max	Min
MgO[1]	7.81	4.83	10.51	3.07	7.14	4.48	10.91	5.38
K$_2$O[1]	0.83	0.36	1.49	0.33	0.88	0.46	1.01	0.02
S[1]	0.24	0.07	0.29	0.06	0.21	0.11	0.24	0.07
Cl[1]	0.38	0.05	0.16	0.02	0.04	0.02	0.04	0.01
Sr	1755	594	533	195	331	291	351	307
Y	43.0	24.3	34.8	14.3	34.3	28.7	31.5	26.1
Zr	274	175	166	62	148	124	177	134
Nb	22.1	10.8	10.2	4.4	12.3	9.3	24.5	15.8
Ba	320	216	754	123	186	142	176	131
La	24.7	15.5	12.6	4.8	10.8	9.2	13.9	9.0
Ce	63.1	48.6	32.2	14.6	32.8	25.5	38.1	26.8
Yb	3.8	1.7	3.5	1.3	3.1	1.8	3.2	2.2
Pb	4.8	2.4	5.1	0.2	2.9	1.8	2.5	1.2
Th	3.0	0.7	2.0	0.4	1.1	0.6	2.6	1.1
U	0.7	0.3	0.9	0.2	0.5	0.3	0.9	0.4

addition, despite overlapping compositions, HFSE (Nb, Ta, and Zr) and LREE (La and Ce) are generally more abundant in arc melt inclusions.

Although young shoshonitic compositions are not observed in the backarc, there is a distinct trace-element enrichment of forearc lavas relative to arc lavas. Despite a more mafic whole rock composition and being trapped within the most fosteritic olivines in this study (Fo_{86-90}), forearc shoshonitic melt inclusions are generally less mafic (6.77 wt% MgO) relative to shoshonitic arc inclusions (7.24 wt% MgO; Tables 8-10). Inclusions from the forearc shoshonitic lava have, on average higher K_2O (2.17 wt% versus 1.95 wt%), lower Na_2O (2.49 versus 3.08 wt%) and significantly greater P_2O_5 (1.33 wt% versus 0.48 wt%). Trace elements are almost universally enriched in forearc shoshonitic melt inclusions relative to arc inclusions, including a 2-3 times enrichment in LREE and MREE concentrations, with the notable exception of a greater depletion in HREE, Y, and Yb in the forearc inclusions (Fig. 21a). Major, trace, and volatile element variability in melt inclusions is summarized for select elements, categorized by sample location (forearc, arc, backarc) and basalt type in Table 10.

Volatile elements

Chlorine and sulfur concentrations in unbreached Oregon Cascade melt inclusions vary markedly both within basalt groups and overall across the arc. As stated previously, melt inclusions have been screened based on chlorine and sulfur abundances following Nielsen et al (1998) such that only inclusions which retain their trapped volatile contents are included in this study. Sulfur concentrations are controlled dominantly by Fe content and sulfur speciation in basaltic magmas, such that increasing Fe content and oxidation

(measured as an increase in percent sulfate) results in greater sulfur solubility (Fig. 22; Wallace and Carmichael, 1992).   In more reduced lavas (> FMQ), the maximum sulfur concentration in melt inclusions is controlled by sulfide saturation therefore no discernable across arc variation is evident in these samples. However, the maximum sulfur concentration of melt inclusions generally increases from the backarc to forearc due to increasing oxygen fugacity resulting in a maximum concentration of 0.57 wt% S in the forearc shoshonitic basalt, double the maximum S concentration observed in the backarc basalts (Fig. 23).

Chlorine concentrations range from essentially degassed to a maximum of 3740 ppm in rehomogenized inclusions. The highest chlorine concentrations are in forearc shoshonitic inclusions and in arc OIB-like inclusions. As with S concentrations, Cl/Ti ratios generally increase across the arc from 0.03 ± 0.01 to 0.16 ± 0.02 (1 σ). Cl/K ratios however show little overall across arc variation, possible as a result of the high mobility of both K and Cl in subduction related fluids (Fig. 24a). LKT lavas have essentially identical Cl/K and Cl/Ti ratios between arc and backarc lavas with an average of 0.08 ± 0.01 and 0.03 ± 0.02, respectively (1 σ). Calc-alkaline basalts are more highly variable between samples but have a similar range in Cl/Ti between backarc (0.15-0.02) and arc (0.12-0.03) melt inclusions. While Cl/K and Cl/Ti ratios in shoshonitic melt inclusions increase from arc to forearc, average Cl/K ratios are similar to those in CAB inclusions (Fig. 23, 24).

Arc OIB-like melt inclusions from WF04-1(WF02-1) have Cl/K and Cl/Ti ratios significantly greater than observed in other arc or backarc OIB-like lavas with a
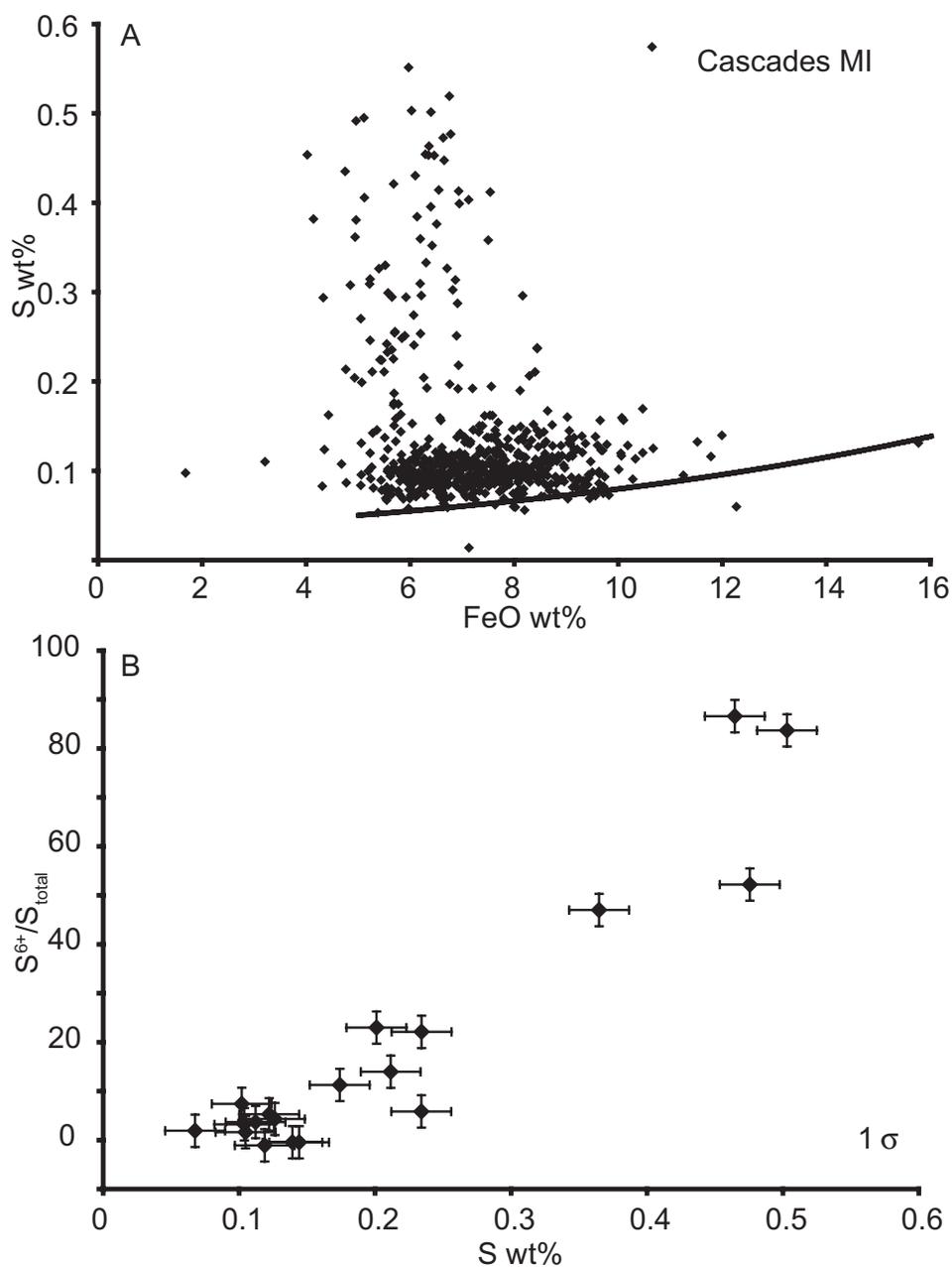
Figure 22. (A) Sulfur concentration (wt%) versus FeO (wt%), calculated assuming an olivine-melt $K_D^{Fe\text{-}Mg}$ of 0.3 (Roedder and Emslie, 1970). Solid line is the Fe-sulfide saturation curve of Wallace and Carmichael (1992), defining the lower limit of sulfur concentrations in rehomogenized melt inclusions. (B) S concentration (wt%) versus sulfur speciation (S^{6+}/S_{total}), depicting the significantly greater solubility of sulfur as sulfate. Error bars for sulfur speciation are 3.5% based on repeat analysis of Galapagos glass K 14-3 (1 σ; Christie et al., 1986).

Figure 23. Melt inclusion (A) Ba concentrations (ppm), (B) Cl/Ti, and (C) S wt% versus sample distance to the trench. Forearc, arc, and backarc basalts are segregated by the vertical dashed lines. High sulfur concentrations (>0.15 wt%) are generally the result of increased oxidation of sulfur in melt inclusions (Fig. 20). Fluid-mobile trace elements, volatiles, and oxygen fugacity (determined from sulfur speciation) all indicate a relative increase closer to the trench. Forearc, arc, and backarc basalts are represented by filled, grey, and open symbols, respectively, while symbol shape denotes basalt classification. Squares, diamonds, circles, and triangles represent shoshonitic basalts, calc-alkaline basalts, ocean-island basalts and low-K tholeiitic basalts, respectively.
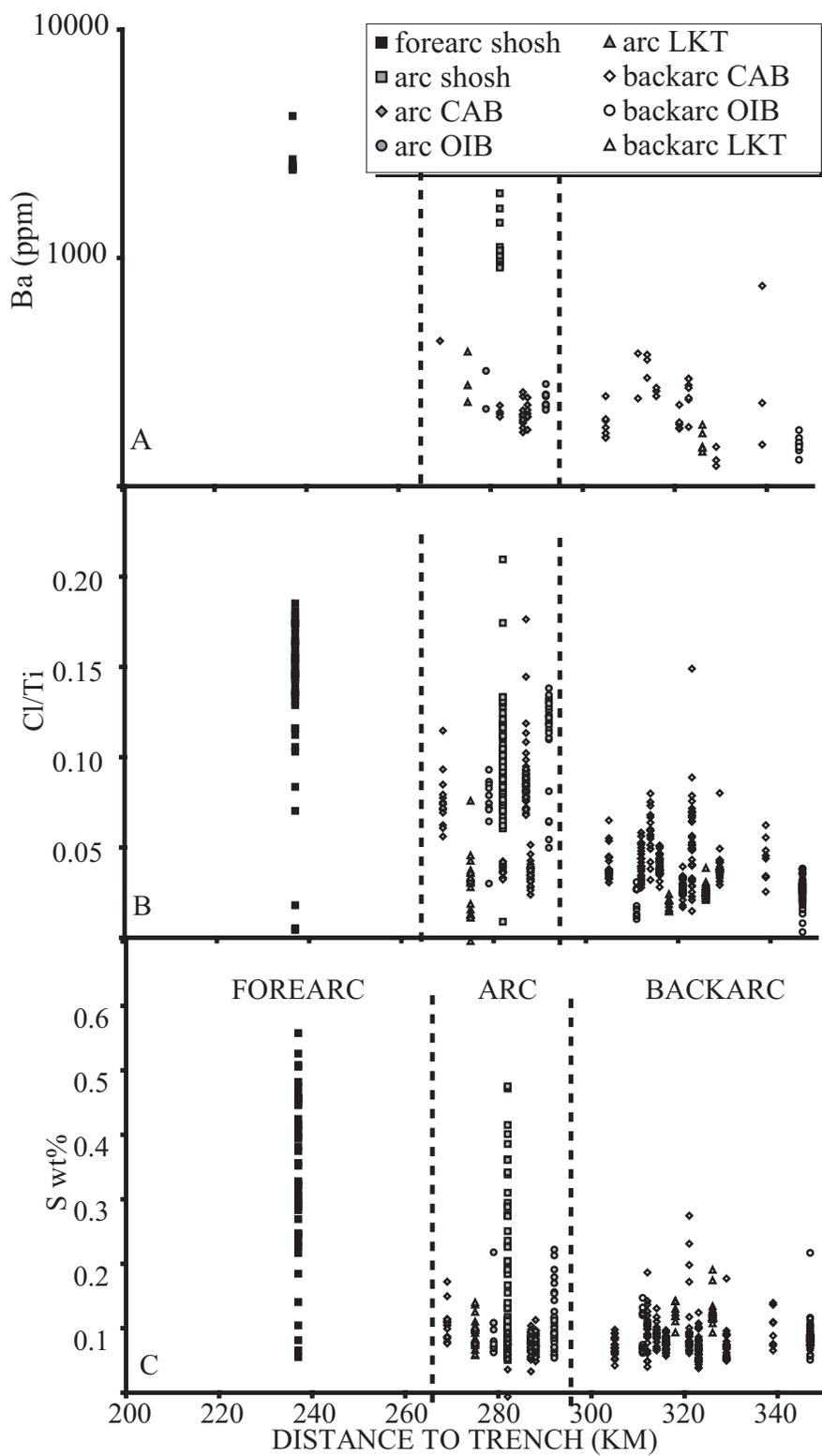
Figure 23.

Figure 24. (A) Cl/K versus Cl wt% illustrating the relative consistency of Cl/K ratios despite a large range in Cl concentrations and the enrichment in Cl concentration in OIB-like basalts. Maximum Cl concentration from an OIB-like lava is 0.38 wt%, denoted by the arrow. Open fields are the range of melt inclusion compositions for backarc lavas. (B). Ba/Nb versus Cl/K for olivine-hosted melt inclusions.   OIB-like basalts have an extreme enrichment in Cl/K relative to other Cascade basalts while lacking a significant Ba/Nb enrichment characteristic of addition of a subduction component (see text). Symbols are the same as Figure 23.
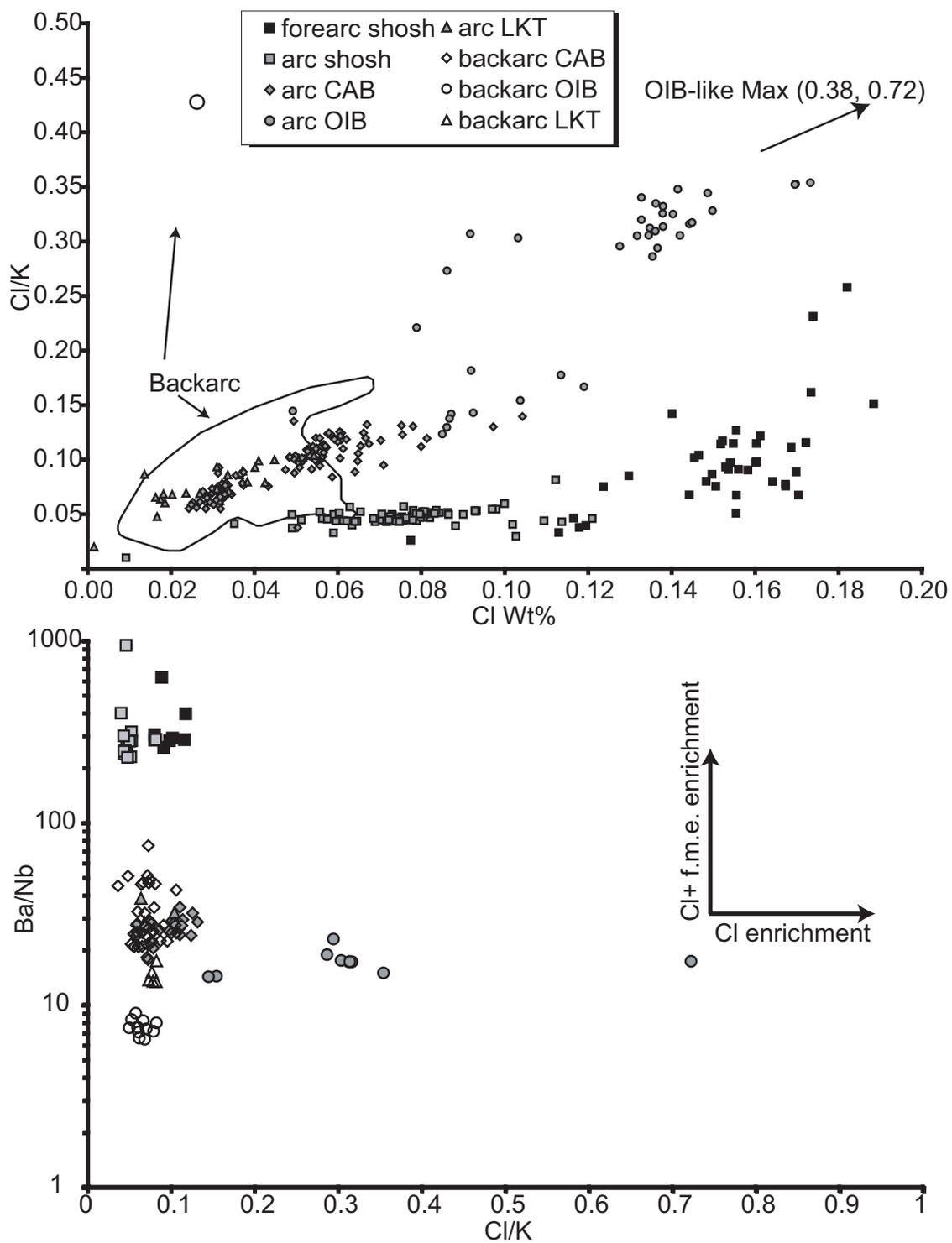
Figure 24.

maximum of 0.72 and 0.22, respectively. The significant increase in Cl relative to K is also true of Cl relative to other fluid mobile elements (Fig. 24). Ba/Nb ratios, typically considered an indicator of slab fluid enrichment, increase from backarc to forearc with little change in Cl/K, however Cl/K ratios in WF04-1 inclusions are significantly greater than other basalts despite Ba/Nb ratios consistent with other arc basaltic melt inclusions (Fig. 24b). Likely sources for a significant Cl enrichment to the primitive OIB-like inclusions are; 1) Cl enriched fluid from the subducting slab and 2) assimilation of a Cl-rich crustal brine. Since Cl in OIB-like inclusions appears to be decoupled from other fluid mobile elements commonly interpreted to be present in a subduction component and since the Cl enrichment appears to be significantly greater than measured in other arc and forearc inclusions it seems unlikely that this apparent Cl over-enrichment occurred as a result of subduction processes. Neither Cl concentrations nor Cl/Ti ratios vary greatly with variations in major elements, although several low SiO_2 (45-47.5 wt%) and high CaO (12.34-13.9 wt%) melt inclusions, distinct from other OIB-like inclusions, have Cl concentrations more consistent with other arc magmas. The overall lack of systematic variation in Cl/Ti with decreasing MgO concentration however suggests that if the Cl enrichment resulted from the assimilation of a crustal brine this likely occurred early in the evolution of the magma, prior to entrapment of melt inclusions in the crystallizing magma.

DETERMINATION OF OXIDATION STATES IN BASALTS

For the shoshonitic, CAB, LKT, and OIB-like basalt groups, one primitive basalt from each group was chosen from the arc, backarc, and for the shoshonitic basalts the forearc, to determine oxygen fugacity (Table 11). In addition to major element and trace element characteristics, basalts were chosen to provide the greatest quantity of large melt inclusions, required for the sulfur Kα peak shift method. The primary method of determining basaltic oxidation state in this study is based on the sulfur speciation of the melt inclusions. Olivine-chromite oxygen geobarometery is utilized as a secondary technique to better evaluate the accuracy of the calculated oxygen fugacity from the measured sulfur speciation. The following discussion summarizes each of the techniques utilized to determine oxygen fugacity and the results obtained from comparing the two methods.

Sulfur Kα peak shift

Based on sulfur speciation (S^{6+}/S_{total}) measurements, oxidation state, reported relative to the FMQ oxygen buffer, can be calculated empirically based on the relationship determined by Wallace and Carmichael (1994; Fig. 25a). A similar empirical curve defined by Jugo et al. (2005) is buffered at higher oxidation states due to an assumed greater significance of sulfite (S^{4+}), resulting in a maximum $X[S^{6+}]$ equivalent of 0.86 (the term $X[S_{6+}]$ equivalent is used by Winther et al (1998) and Jugo et al (2005) to indicate a relative change in speciation rather than a strict determination of S^{6+}/S_{total} as a result of the presence of sulfite). While sulfite has been identified in highly oxidized melt inclusions the maximum reported proportion is only 16% with a relative error of 20%, and does not appear to vary systematically with either percent sulfate or

Table 11: Summary of calculated oxygen fugacity for Cascade basalts.

Sample[1]	QV	WF	CC	FLR	CM	TB	NEF	BLW
Log fO$_2$ (ΔFMQ)-S Kα[2]								
Average	1.91	0.28	-0.06	-0.24	1.16	<-0.25	<-0.25	<-0.25
+/-[4]	0.05	0.34	0.26	--	0.06	--	--	--
High	1.96	0.62	0.13	0.07	1.2	<-0.25	0.38	-0.17
Low	1.86	-0.08	-0.24	<-0.25	1.11	<-0.25	<-0.25	<-0.25
Log fO$_2$ (ΔFMQ)-Olivine-Chromite 1 kbar[3]								
Average	1.50	0.88	0.35	0.44	1.28	0.58	0.99	0.38
+/-[5]	0.23	0.12	0.43	0.46	0.14	0.19	0.10	0.15
High	1.83	0.99	0.99	1.45	1.53	0.90	1.06	0.59
Low	1.12	0.66	-0.37	-0.25	1.06	0.36	0.92	0.13

[1]Sample prefixes correspond to sample numbers from Table 7. [2]average and 1 standard deviation calculated after Wallace and Carmichael (1994); inclusions undergoing degassing and post-entrapment modification are not included. [3]Oxygen fugacity calculated after Ballhaus et al. (1990). [4]1 standard deviation from average of multiple analyses when all peak shift measurements have a calculated oxygen fugacity greater than -0.25 log units (ΔFMQ). [5]1 standard deviation from average of multiple olivine-chromite pairs.

Figure 25. A) Sulfur speciation versus $\log fO_2$ relative to the fayalite-magnetite-quartz oxygen buffer (FMQ) for empirical curves of Wallace and Carmichael (1994), abbreviated WC, and Jugo et al. (2005). Shaded field around the Wallace and Carmichael (1994) curve defines an upper and lower error limit based on an error of 3.5% S^{6+}/S_{total} from standard reproducibility. Dashed boundaries at -0.25 and +2.57 define the limit of $\log fO_2$ (ΔFMQ) that can be accurately determined (see text for more details). B) Comparison between $\log fO_2$ (ΔFMQ) calculated from Wallace and Carmichael (1994) and Jugo et al. (2005). The Jugo et al (2005) curve deviates from the Wallace and Carmichael (1994) curve with a maximum S^{6+}/S_{total} of 0.86.
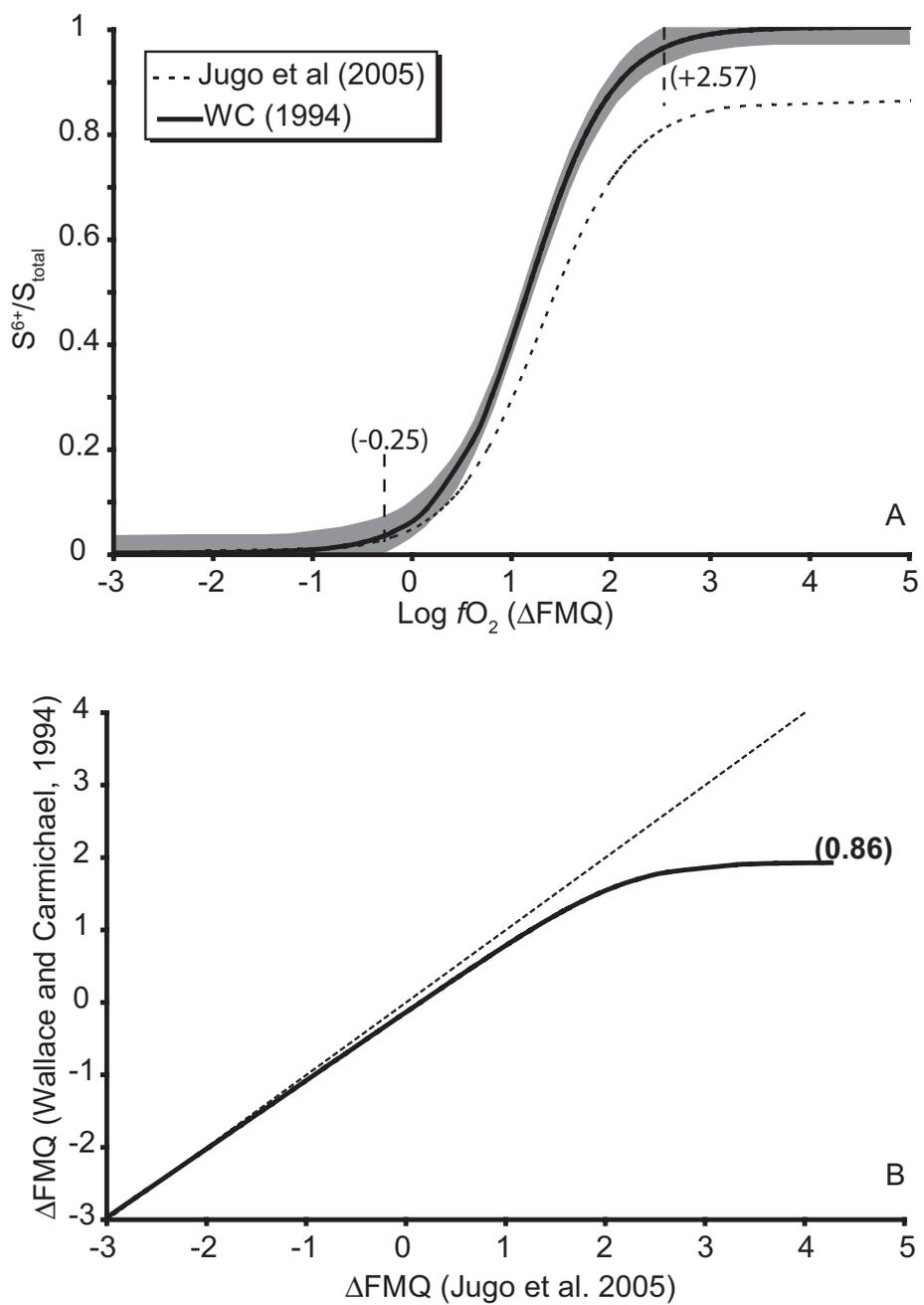
Figure 25.

total sulfur concentration (Metrich et al., 2002). Since the significance and variability of sulfite in basaltic melts is still not well constrained and because at low fO_2 the Wallace and Carmichael (1994) and Jugo et al (2005) curves correspond reasonably well, we have maintained the use of the Wallace and Carmichael (1994) curve to determine oxidation state from sulfur speciation (Fig. 25b).

The asymptotic relationship between sulfur speciation and fO_2 at very low and high percent sulfate, coupled with an estimated reproducibility of $\pm 3.5\%$ sulfate, defines the lower and upper limits for determination of fO_2 from sulfur speciation at -0.25 log units (ΔFMQ) and +2.57 log units (ΔFMQ), respectively (Fig. 25a). In strict use, the limits for reliable estimation of oxidation state are between FMQ and ~2.3 log units above FMQ, similar to those suggested by Jugo et al. (2005), since at oxidation states outside this range, errors in estimating fO_2 become unreasonably large. Therefore, when the proportion of sulfate is below 4% or above 96% an independent means of estimating fO_2 is required.

Degassing of the melt during entrapment and post-entrapment modification of the melt inclusion can significantly alter the sulfur speciation and oxidation state of the inclusion (Chapter 2; Danyushevsky et al., 2002; Metrich et al., 2005; Mathez, 1984). Depending on the initial oxidation state and water content of the melt, degassing can result in either an oxidation or reduction of the melt. As SO_2 is the dominant sulfur gas species during degassing of basaltic magmas, the sulfur speciation can be modified by either the reduction of S^{6+} or the oxidation of S^{2-}, depending on the initial oxidation state

and water content of the melt (Chapter 2; Carrol and Webster, 1994; Wallace and

Carmichael, 1994; Anderson and Wright, 1972).

Post-entrapment modification of the trapped melt by either hydrogen diffusion or

Fe-loss will result in the oxidation of the inclusion (Danyushevsky et al., 2002). Fe-loss

during re-equilibration of a melt inclusion will increase the Fe^{3+}/Fe^{2+} of the melt.

Depending on the initial Fe concentration and Fe^{3+}/Fe^{2+} ratio, the resulting change in

oxidation state will vary. For example, a typical CAB composition (CC02-1)

experiencing ~1.2 wt% Fe-loss will result in an increase in fO_2 of only ~0.22 log units.

The decrease in the FeO content of the melt may also result in the precipitation of sulfide

globules, further increasing the S^{6+}/S_{total}, since the concentration of dissolved sulfur as

sulfide is strongly dependant on iron content (Danyushevksy et al., 2002).

Rapid diffusion of hydrogen out of melt inclusions is commonly observed in

inclusions which have been slowly cooled or have been kept at high temperatures for an

extended period of time (Hauri, 2002; Qin et al, 1992). As a result of hydrogen diffusion,

excess oxygen is retained within the melt inclusion causing the melt to oxidize

(Danyushevksy et al., 2002; Rowe et al., 2006). As hydrogen diffusion progresses, the

calculated olivine-melt K_D^{Fe-Mg} will become larger with increasing oxidation due to the

overestimation of Fe^{3+} as a result of the higher fO_2 (Chapter 2). Melt inclusions from

both arc and backarc CAB lavas included in this study for which sulfur speciation was

determined appear to have undergone hydrogen diffusion resulting in a wide range of

calculated oxidation states. For these CAB lavas, only the inclusions with lowest percent

sulfate that are the closest to being in equilibrium (K_D^{Fe-Mg} of ~0.3) with their respective

host olivine grains are reported in this study. Multiple sulfur speciation measurements from a single sample are therefore required to distinguish inclusions which have been affected by degassing and post-entrapment modification however, once these critical variables have been accounted for, sulfur speciation does produce a reliable estimate of magmatic fO_2 at the time of melt inclusion entrapment.

Chromite-olivine oxygen geobarometry

Compositions of chromite inclusions within olivine phenocrysts provide a secondary means of estimating magmatic oxidation states based on the redox equilibrium reaction:

$$6Fe_2SiO_{4(olivine)} + O_{2(melt)} = 3Fe_2Si_2O_{6(orthpyroxene)} + 2Fe_3O_{4(spinel)} \qquad \text{equation 1}$$

Oxygen fugacity is calculated following the method of Ballhaus et al. (1990). Although this method requires the compositions of olivine, orthopyroxene and spinel equilibrium phases, the orthopyroxene component may be removed through the reaction of orthopyroxene = olivine + SiO_2. In orthopyroxene undersaturated magmas therefore, a correction for the activity of silica (αSiO_2) must then be applied, estimated from Ghiorso and Carmichael (1987), resulting in a reduction of the fO_2 by 0.23 to 0.3 log units (Ballhaus et al., 1991). The advantage of utilizing this technique is that oxidation state may potentially be determined independently of the S peak shift technique within the same olivine grain.

Since chromite inclusions were not always present in olivine grains from which sulfur speciation was measured, multiple chromite inclusions were analyzed from the same grain mounts to provide the most direct comparison. However, because of the

potential for re-equilbration between the host olivine and chromite inclusions at the high furnace temperatures required for melt rehomogenization, oxidation states were calculated from heated and unheated olivine-chromite pairs from three samples spanning the range of oxidation states measured in this study (Kamenetsky et al., 2001; Clynne and Borg, 1997; Scowen et al., 1991; Ozawa, 1984). Calculated oxygen fugacities from heated and unheated melt inclusions correlate within error (1σ), suggesting that little re-equilibration is occurring during the short rehomogenization time (Fig. 26b). This however does not indicate whether sub-solidus re-equilibration has occurred after entrapment of chromite grains within the olivine host prior to eruption or during cooling (see discussion below). Precision of this method is ±0.41 log units at oxygen fugacities above FMQ and ±1.2-1.5 log units approximately 2 log units below FMQ (Ballhaus et al., 1991). Standard deviation (1σ) of multiple chromite-olivine fO_2 estimates are significantly lower than calculated precision, ranging from 0.1 to 0.46 log units (Table 11).

Basalt oxygen fugacity

Correlating fO_2 between chromite-olivine pairs and sulfur speciation is problematic at low fO_2 as a result of our inability to accurately determine oxidation state from sulfur speciation below ~4% sulfate (-0.25 log units below FMQ) despite measured sulfur speciations of essentially 0% sulfate. Chromite-olivine oxygen barometry is also problematic at low fO_2 as a result of errors in determination of ferric iron in spinel from microprobe analysis and the increased imprecision at low fO_2 (Ballhaus et al, 1991; Parkinson and Arculus, 1999). At high oxygen fugacities (>FMQ) calculated oxidation

Figure 26. (A) Chrome no. of chromites as inclusions in olivine grains versus calculated oxygen fugacity (ΔFMQ) based on the method of Ballhaus et al. (1990). Cr no. and spinel compositions are calculated with a spreadsheet provided by M. Clynne. Also plotted are mantle peridotite spinels from Parkinson and Arculus (1999) and Brandon and Draper (1996). Spinels from Simcoe volcano, WA (Brandon and Draper, 1996), have calculated oxygen fugacities comparable to the range observed in Oregon Cascade basalts although do not correlate with the high fO_2, high Cr no. forearc spinels. (B) Calculated oxygen fugacity for unheated and heated chromite-olivine pairs indicating that there is no evidence for significant re-equilibration during rehomogenization of melt inclusions. Error bars are based on variation from multiple analyses (1 σ).

147
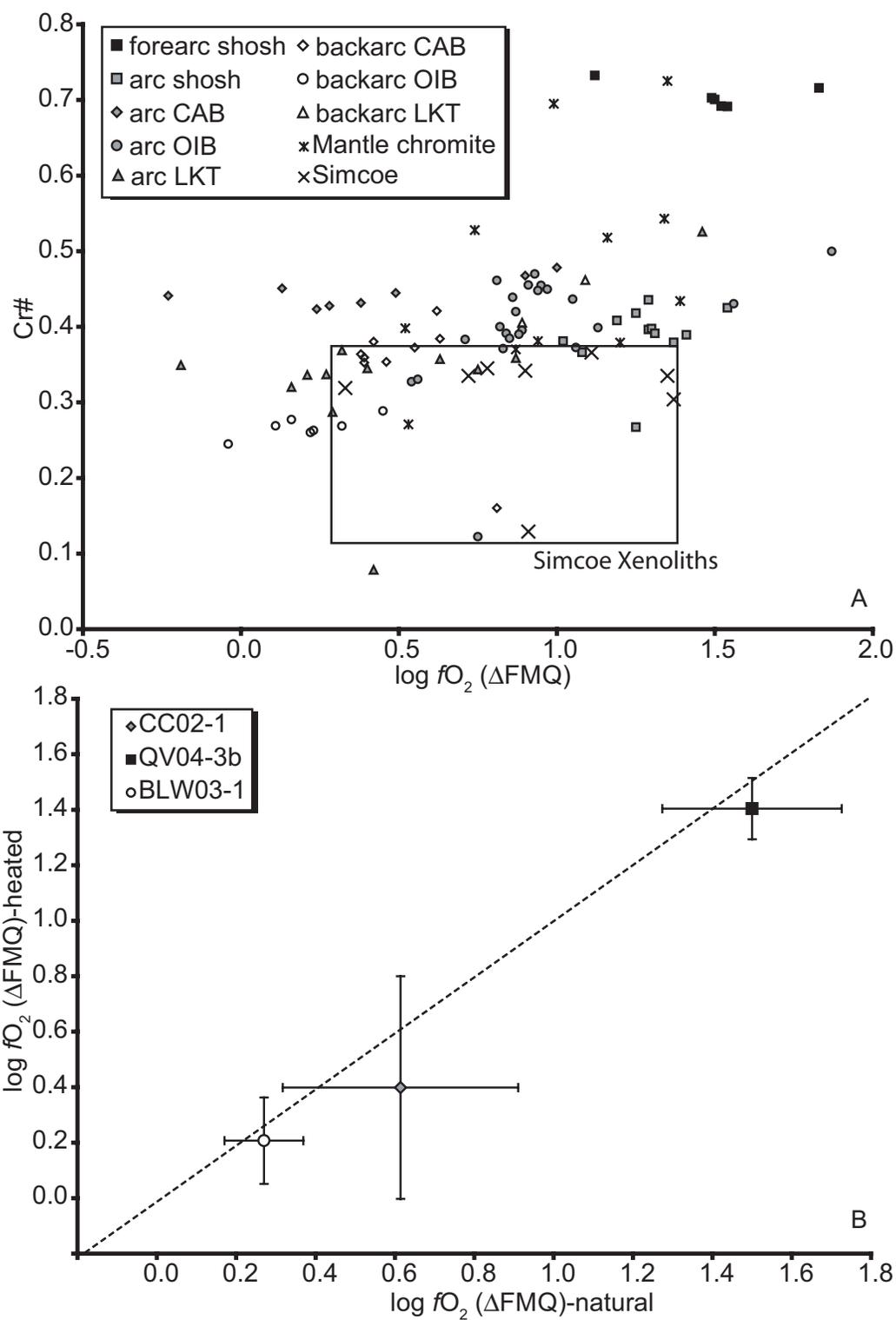
Figure 26.

states from sulfur speciation and olivine-chromite oxygen geobarometery correlate

reasonably well, however at low fO_2 (<FMQ) oxygen fugacities calculated from

chromite-olivine pairs are typically greater than predicted by sulfur speciation by as much

as 1.25 log units (Fig. 28). Although there is no evidence to suggest re-equilibration of

chromite and olivine pairs during melt inclusion rehomogenization, re-equilibration may

have occurred naturally as a result of slower cooling (Kamenetsky et al., 2001; Barnes,

1998; Scowen, et al., 1991). This re-equilibration is likely to have occurred in the LKT

(NEF03-1 and FLR03-1) and backarc CAB (TB03-1) lavas which were collected further

from estimated vent locations in relatively thick flows. As a result of the inherent

problems associated with determination of low oxygen fugacities and because of the

potential for olivine-chromite re-equilibration, we feel that estimates based on sulfur

speciation measurements provide a better approximation of the primitive basaltic fO_2.

Based on sulfur speciation measurements, calculated oxygen fugacities for basalts

from across the Cascade arc are highly variable ranging from <-0.25 to +1.9 log units

(ΔFMQ; Fig. 25; Table 11). OIB-like basalts, LKTs, and CABs have relatively similar

calculated oxygen fugacities varying from <-0.25 to +0.28 log units (ΔFMQ). Oxidation

states calculated for OIB-like arc melt inclusions are, on average ~0.5 log units greater

than OIB-like backarc inclusions (Table 11). Arc calc-alkaline melt inclusions have a

slightly higher average oxidation state relative to backarc CAB inclusions, however are

still within 1σ standard deviation of each other. Low-K tholeiitic inclusions from the arc

lava have oxidation states indistinguishable from the backarc LKT melt inclusions (Fig.

28). In addition to the greatest across arc variability, shoshonitic inclusions are
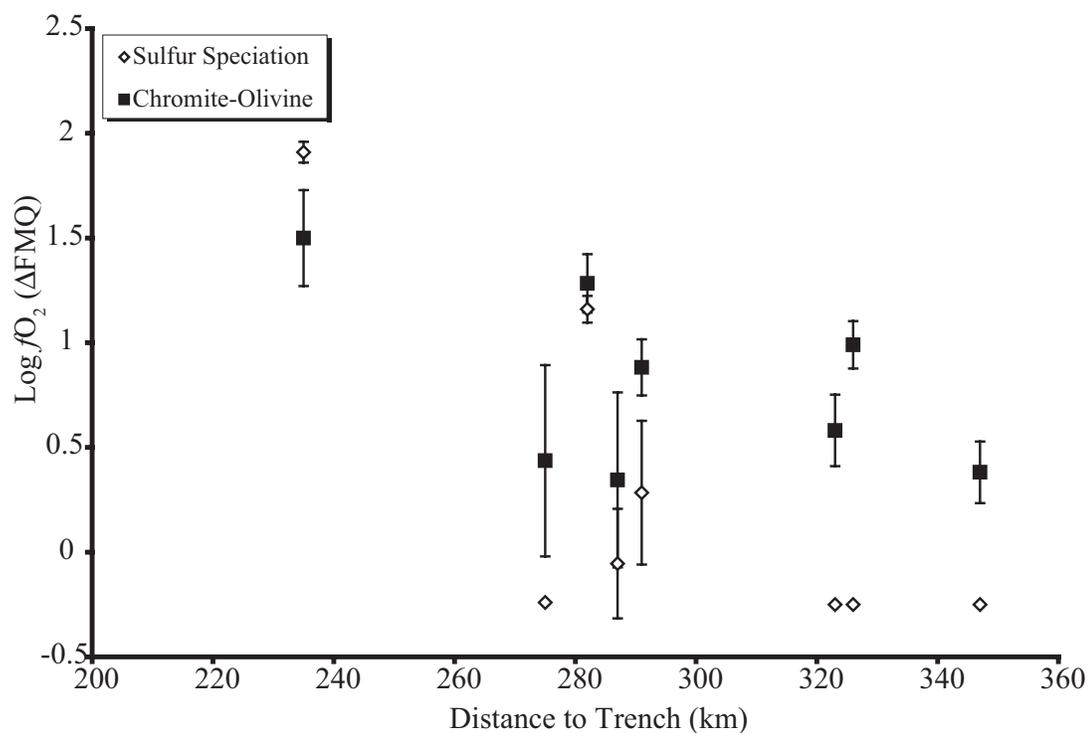
Figure 27. Calculated oxygen fugacities from both sulfur speciation and chromite-olivine pairs as a function of distance to the trench. Oxygen fugacity values are averages reported in Table 11. Error bars are variability in calculated fO_2 (1 σ). Oxygen fugacity based on sulfur speciation measurements without error bars are at or below -0.25 log units (ΔFMQ) and cannot be precisely determined (see text).
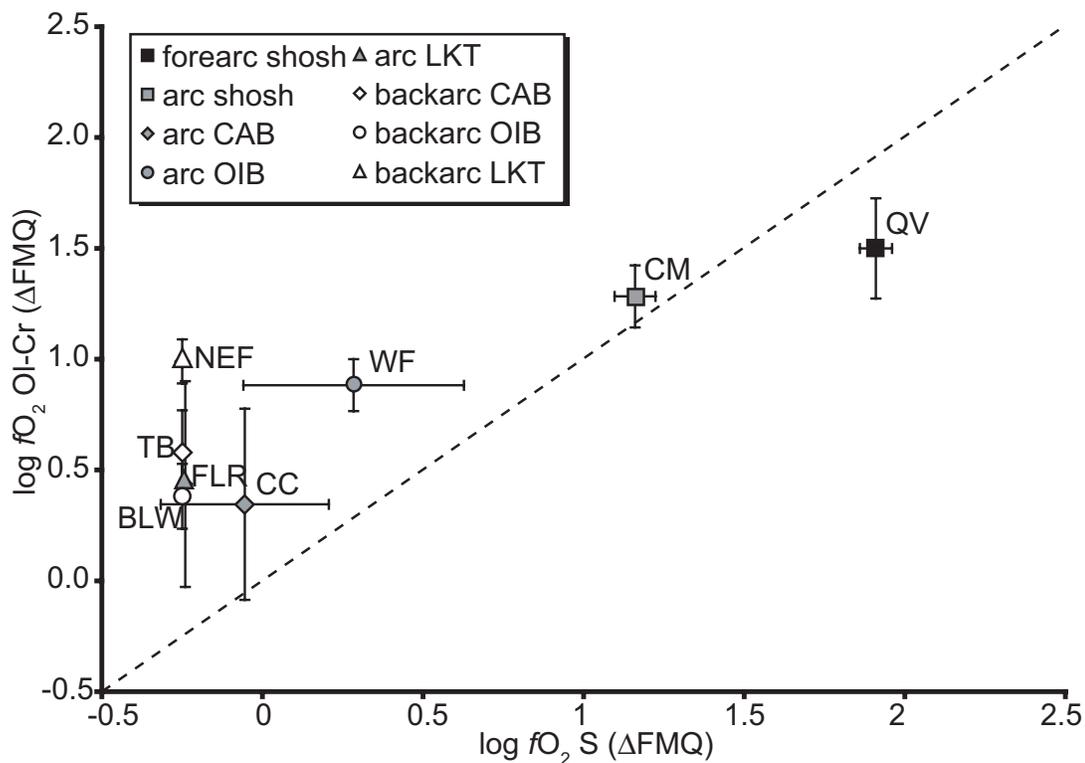
Figure 28. Average log fO_2 (ΔFMQ) determined from chromite-olivine pairs (Ballhaus et al., 1990) versus sulfur speciation in melt inclusions (Wallace and Carmichael, 1994). Labels on points correspond to sample prefixes (Tables 7, 11). Oxygen fucagities correlate well at higher oxidation states however at oxidation states below FMQ (based on sulfur measurements) fO_2 determined from chromite-olivine pairs are up to 1.25 log units higher. All samples with measured sulfur speciation less than lower limit of fO_2 determination are plotted at the lower limit of -0.25 log fO_2 S (ΔFMQ). For samples with one or more analyzed melt inclusions with sulfur speciation beyond the limit of oxygen fugacity determination no error bars are plotted; all other error bars are 1 σ.

significantly more oxidized, with fO_2 from +1.16 to +1.91 log units (ΔFMQ), with the highest measured oxygen fugacity from the forearc shoshonitic lava (Fig. 28). The distinction between oxidation states of shoshonitic basalts and LKT, CAB and OIB-like basalts in conjunction with the overall decrease in basaltic fO_2 from forearc to backarc in the Oregon Cascades suggests that the variations in oxidation states of the basaltic magmas are likely the result of multiple variables related to basalt distribution across the arc and basalt petrogenesis. Despite overall variations resulting from differences between basalt groups, basaltic fO_2 estimated by chromite-olivine pairs and from sulfur speciation indicate a general increase in oxidation state from the backarc to the forearc of the Oregon Cascades (Fig. 27).

SUBDUCTION INFLUENCE ON BASALT OXIDATION

Correlation of fO_2 and trace elements

Identification and interpretation of the effects of addition of an enriched melt/fluid (i.e. subduction component) on the generation of subduction zone magmas has been the focus of numerous volcanic arc studies (i.e. Grove et al., 2003; Churikova et al., 2001; Hochstaedter et al., 2001; Stolper and Newman, 1994). Correlating trace- and volatile-element concentrations with sulfur speciation and oxygen fugacity for over 100 km across the Oregon Cascade volcanic arc however allows us to directly examine the effects of a subduction component on the oxidation states of basaltic magmas as a function of distance to the trench and basalt geochemistry and petrogenesis (Fig. 23, 29).

Figure 29. Sulfur speciation versus (A) Sr, (B) Ce, (C) Ba, and (D) Cl/K for melt inclusions. Figures A-C indicate an increase in fluid-mobile elements with increasing oxidation consistent with the suggestion that oxidation occurs as a result of addition of a subduction component rich in fluid-mobile elements. Cl/K ratios increase in OIB-like melt inclusions without significant change in sulfur speciation, similar to Figure 24, again suggesting Cl is decoupled from other trace elements (see text).
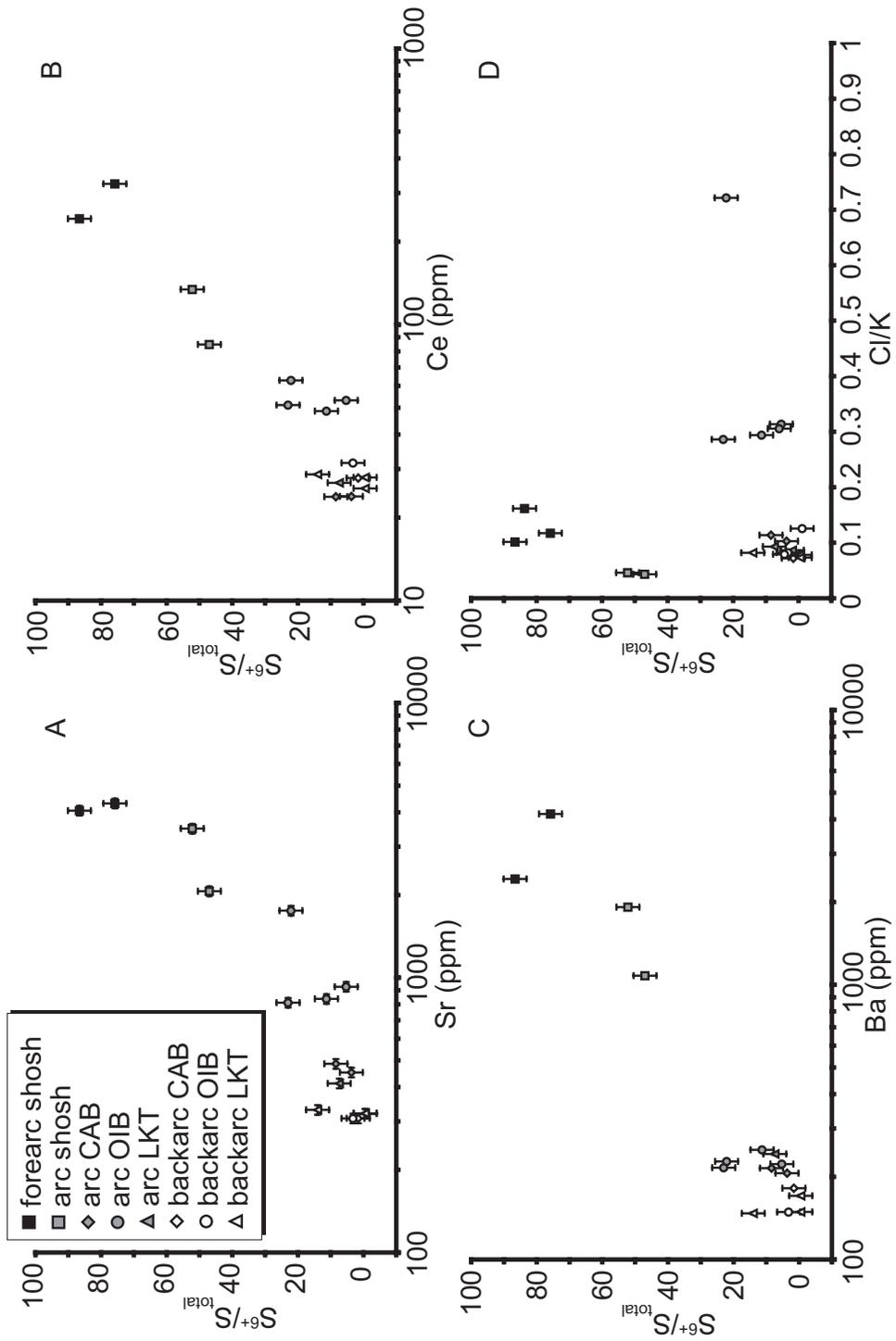
Figure 29.

Overall in the Oregon Cascades there is a clear correlation between fluid-mobile elements (LILE and LREE) and sulfur speciation, with LILE and LREE concentrations increasing at higher oxidation states (higher percentage sulfate; Fig. 29) As previously discussed, concentrations of fluid-mobile trace elements such as Sr and Ba generally increase from backarc to arc to forearc (Fig. 23). These observations suggest that the increase in fluid-mobile elements and basalt oxidation state are the result of the increased influence of a subduction component nearer to the trench, also consistent with the general increase in Cl/Ti towards to forearc (Fig. 23b).

While OIB-like basalts and shoshonitic basalts have a clear enrichment in fluid-mobile elements and increase in oxidation state from backarc to arc, and arc to forearc, respectively, CAB and LKT basalt correlations between fO_2, trace-element geochemistry and distance to the trench become more complicated. Sulfur speciation and fO_2 of backarc lavas are essentially indistinguishable between basalt groups, typically with oxidation states below the FMQ oxygen buffer.   The lack of significant variation in either CAB or LKT compositions as previously depicted between the backarc and arc, either in terms of oxygen fugacity or trace element concentrations (Fig. 21, 28), suggests that 1) the LKT basalt group is not significantly affected by a subduction component derived from the subducting Juan de Fuca plate and that 2) the trace element signature of the CAB lavas may not be related to the current subduction as has previously been suggested (Leeman et al., 2005).

An important observation regarding the increased sulfur oxidation from backarc to arc in the OIB-like inclusions is that the decoupling of Cl from fluid-mobile trace

elements observed in the arc OIB-like inclusions is also true of sulfur speciation and Cl concentration. Figure 29 illustrates that fluid-mobile elements (La, Ba, Sr) in the arc OIB-like inclusions increase as a function of $f\mathrm{O_2}$ similar to other Cascade basalts, however the high Cl/K ratios are anomalous with regard to sulfur oxidation. This observation supports prior arguments that despite decoupling of Cl from other trace elements, increasing concentrations of fluid-mobile elements and higher oxidation states from backarc to arc in OIB-like inclusions is consistent with the increased addition of a slab component closer to the trench.

Flux melting

In order to better constrain the influence of a subduction component to the oxidation states of basalts we must first determine the amount of subduction component added to the mantle source. Decompression melting and flux melting are considered here as two main endmember mantle melting models in subduction zones. The relative significance of either melting scenario is strongly dependent on the subarc thermal structure, rate of subduction, and temperature of subducting slab (Schmidt and Poli, 1998; Davies and Stevenson, 1992). For hot subduction, such as the Cascadia subduction zone, dehydration of the subducting slab occurs at relatively shallow depths, and as a result, flux melting may be of relatively lesser significance (Harry and Green, 1999, Leeman et al., 2005).

Despite the potential greater importance of decompression melting, flux melting of the subarc mantle has significant advantages for modeling of subduction zone magmatism. The paired relationship between the amount of subduction component

added to the mantle and the degree of melting (%F) provides reasonable approximations

of both parameters while reducing the number of unconstrained variables (i.e. Stolper and

Newman, 1994; Reiners et al. 2000). In addition, trace-element signatures characteristic

of OIB-like, LKT, and CAB magmas can be generated from a single enriched mantle

source by varying temperature, %F, and wt% subduction component, from OIB-like

melts (low %F, low SC input) to CAB melts (highest %F and greater SC input; Fig. 30,

12; Reiners et al., 2000). While we do not dispute the likelihood of decompression

melting of a variably subduction-enriched mantle source, changing the melt model does

not significantly impact our estimates or the relative differences of melting conditions

between basalt groups.

We have used an isenthalpic (heat balanced) flux melt model, similar to Reiners et

al (2000) in the Central Washington Cascades, to constrain degree of melting and amount

of subduction component added to the mantle. While the amount of melting increases

with increasing SC, for isenthalpic melting, the generation of melt consumes heat thereby

reducing the mantle temperature. The result is that as melting progresses the efficiency

of the subduction component to generate melt decreases (see figure 6 of Reiners et al

2000) such that a greater amount of subduction component must be added to generate the

same increment of melt. Initial addition of a subduction component generates melts

which are compositionally similar to OIB-like melts and as melting increases melt

compositions resemble LKT magmas. Eventually enough subduction component must be

added to continue melting the peridotite that the composition of the subduction

Figure 30. (A) Ba, (B) Sr, and (C) Ce versus Nb from Cascade melt inclusions. Solid curves are flux melting from 1250°C to 1500°C of a peridotite source (Reiners et al, 2000) similar to the Borg et al (1997) OIB source (Table 12). Plus signs are increments of 5% melting. Maximum flux melting is 30%. Dashed line is a batch melting curve with 2% SC (Reiners et al. 2000) added to the Borg et al (1997) MORB source, from 1% to 30% melting.
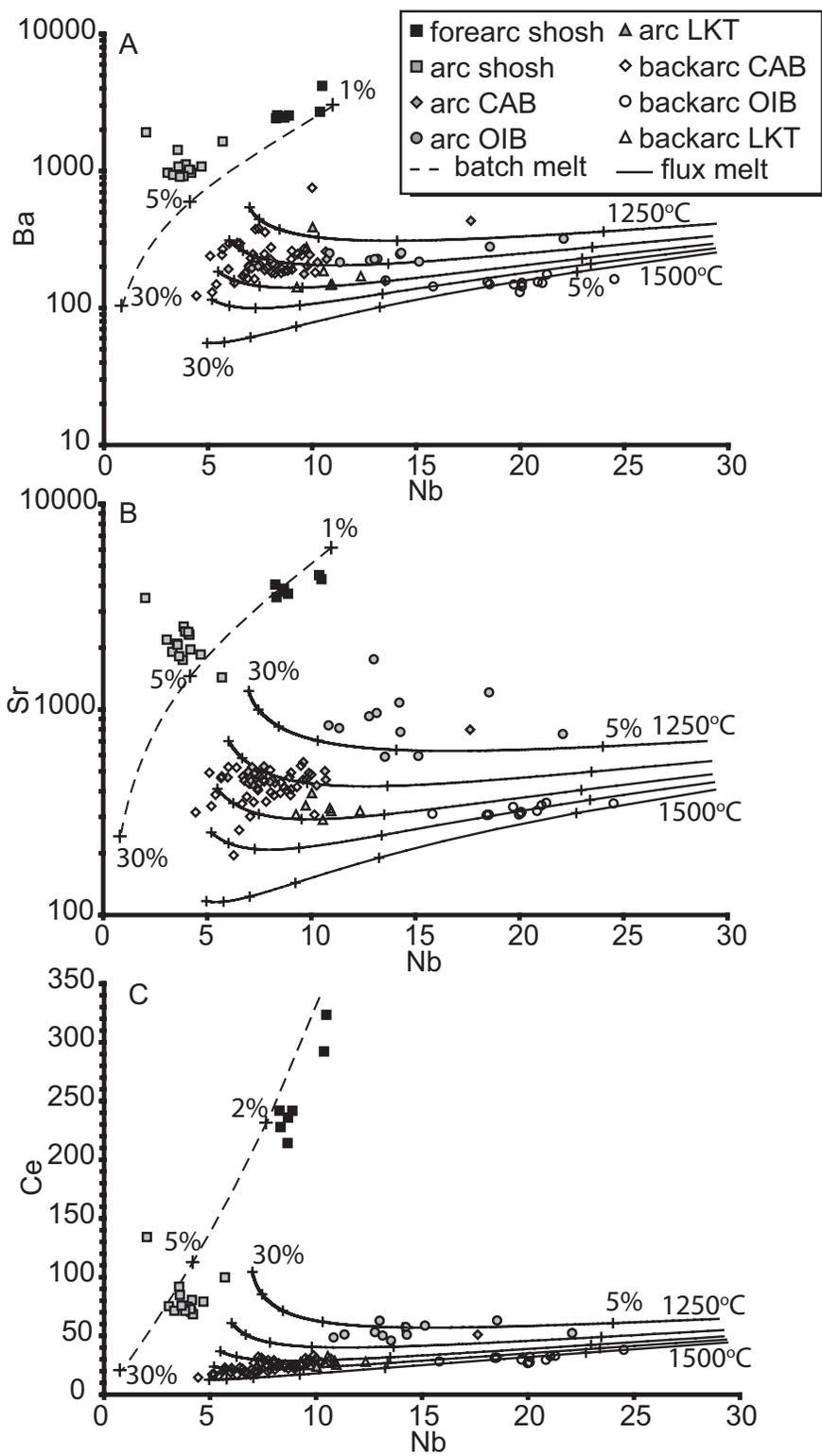
Figure 30.

component begins to exert greater control on the composition of the magma generating

melts compositionally similar to CAB magmas.

Using the peridotite source (similar to the OIB source of Borg et al., 1997) and

subduction component of Reiners et al. (2000) and partition coefficients from Borg et al

(1997), flux melting curves in Figure 30 allow for approximation of T, %F, and %SC

required to generate the basaltic compositions (Table 12). Because of the coupling

between T, F, and %SC in the flux melt model, by estimating the temperature and degree

of melting graphically, the amount of subduction component can be determined from

numerical calculations (see Appendix F for flux melting results). The %F and % SC

added to the source increases from OIB-like (7-10% melt, 0.16-1.48% SC), to LKT (12%

melt, 0.58% SC), to CAB magmas (25-22% melt, 3.78-2.91% SC; averages based on best

estimates from Fig. 30 for backarc and arc basalts, respectively).

Neither flux melting nor simple batch melting of a variably subduction-modified,

peridotite source similar to that used to model CAB, LKT, and OIB-like magmas can

reasonably reproduce the shoshonitic compositions, requiring a significantly different

source composition. However, using the Borg et al (1997) MORB source as a depleted

mantle source, the shoshonitic basalts can be reasonably reproduced with a modal, flux

melt or simple batch melt (Fig. 30; Table 12). High spinel Cr#'s for the Cascade forearc

shoshonitic basalt are also consistent with shoshonitic melt derivation from a depleted

source (Fig. 26a). Cr-rich spinel compositions are comparable to those observed in high-

Mg andesites from the Mt. Shasta and Lassen region in northern California, indicating the

Table 12: Endmember components for flux melt models.

Component[1]	Depleted Mantle	Enriched Mantle	SC
Cs	0.0003	0.00465	3.5
Rb	0.026	0.413	120
Ba	2	9	1500
Th	0.006	0.07	13
U	0.0025	0.02	5.3
Nb	0.32	1.5	8
Ta	0.0075	0.14	0.05
K	27.7	283.85	45000
La	1	0.815	99
Ce	0.49	2.47	297
Pb[2]	0.029	0.17	17
Sr	5.77	18	3500
Nd	0.654	1.4	130
Sm	0.293	0.35	35
Zr	7.2	25	500
Hf	0.2	0.4	20
Eu	0.119	0.13	9
Ti	996	1000	30000
Gd	0.467	0.45	30
Yb	0.402	0.5	12
Cl[3]	4	4	11500

Notes: [1]Depleted source is MORB source of Borg et al (1997), enriched source is peridotite source of Reiners et al (2000), and subduction component (SC) is from Reiners et al (2000). [2]Pb for enriched source from Borg et al (1997) OIB source. [3]Cl from Kent et al (2002).

forearc shoshonitic basalt may have been derived from a mantle source which had previously experienced 20-30% melting (Clynne and Borg, 1997; Baker et al. 1994).

Olivine and orthopyroxene proportions in the depleted peridotite are similar to depleted harzburgite xenoliths recovered from Simcoe Volcano, Washington (Brandon and Draper, 1996). In addition, ~4% garnet and 6% amphibole have been added to the source composition while clinopyroxene is thought to be absent as a result of previous depletion. The presence of residual garnet is indicated by a strong depletion in HREE's and Yb while a hydrous phase (amphibole or phlogopite) is necessary for generating the high estimated water contents.

Batch melting calculations require between 2-5% subduction component added to the depleted peridotite source and the generation of a low degree partial melt (~2-5%; Fig. 30). Flux melting of the depleted source requires a low temperature (~1075°C), similar to a liquidus temperature of ~1115°C determined experimentally for the forearc shoshonitic basalt (Rowe et al., 2006), and addition of ~6 % SC resulting in the generation of 5.8% partial melt. Arc shoshonitic compositions are best fit with a higher initial temperature (~1175°C), less addition of a SC (~2.5%) and higher degree melting (7.6%). While the solutions of flux melt models presented here are non-unique, a more rigorous investigation of melting models is beyond the scope of this study. Estimations presented here from flux melt modeling however provide reasonable approximations of relative differences in %F and %SC between basalt groups across the arc.

Temperatures at which mantle melts have segregated from their respective sources have been independently estimated using the Sugawara (2000) geothermometer

following the method of Leeman et al. (2005; see later discussion).   Based on an empirical fit to molar MgO content and pressure the advantage of this calculation is that temperatures may be estimated independent of melt oxygen fugacity and it is applicable to a wide range of basaltic compositions (Sugawara, 2000). In addition, the Sugawara (2000) temperature estimates are not greatly impacted by moderate uncertainties in pressure, with a temperature difference of ~5.5°C/kbar. Hydrous, olivine saturated basalts are estimated to reduce the segregation temperature by ~5.4°C per mole % H_2O, producing a maximum decrease in temperature of ~90°C below that predicted by the Sugawara model for shoshonitic compositions (based on ~5.5 wt% H_2O estimated by difference from QV04-3b inclusions). Similarly, Leeman et al (2005) predict a reduction of 20°C per 1 wt% H_2O based on the application of the Sugawara (2000) geothermometer to experimental studies of hydrous basalts. Regardless of the potential uncertainties resulting from water content, calculated temperatures provide an estimated maximum temperature for melt segregation, and correspond well with average temperature estimates from flux melting calculations (Fig. 31b).

No correlation between calculated fO_2 and %F is evident from flux melting calculations (Fig. 31a), suggesting that the degree of melting does not significantly influence the oxidation state of the basaltic melt. Similarly, a recent study by Bezos and Humler (2005) has suggested that partial melting processes may be open to oxygen, and as such, the degree of partial melting therefore would not significantly impact the oxidation state of the originally generated magma.

Figure 31. (A) Calculated oxidation state (from sulfur peak shift) versus the approximated weight percent of added subduction component to the mantle source region based on flux melt modeling (Reiners et al., 2000). CAB compositions (TB and CC) lie off a trend of increasing oxidation state with increasing subduction component and may represent re-equilibration with a more reduced mantle source. Prefixes correspond to samples in Table 7, numbers in parentheses are the estimated percent melting required to best approximate the average inclusion compositions (see text). (B) Melt Segregation temperature versus calculated oxidation state. Temperatures for OIB-like, LKT, and CAB compositions from Sugawara (2000) after Leeman et al (2005). Shoshonitic temperatures estimated from flux melt modeling. Inset: Correlation between temperatures calculated with the Sugawara (1 σ) geothermometer and estimated from flux melt modeling (Shoshonitic inclusions excluded as a result of the over-estimation of segregation temperatures due to higher water concentrations).
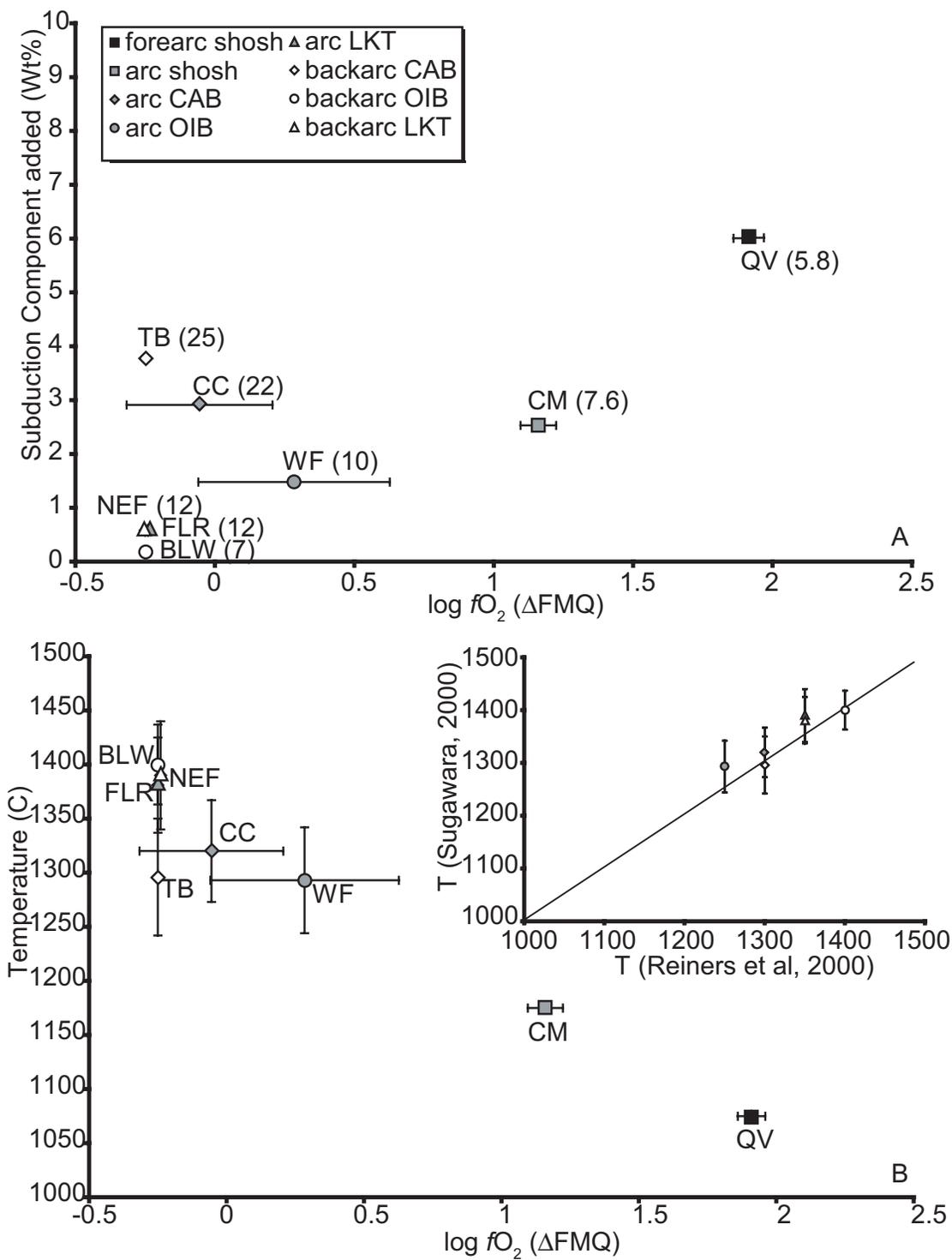
Figure 31.

Reasonable correlations are evident when comparing the estimated melt segregation temperatures and %SC to oxygen fugacity (Fig. 31). As the amount of subduction component added to the mantle source increases, the oxidation state of the magma also increases in LKT, OIB-like and shoshonitic basalts (Fig. 31a). The CAB magmas, which also form from the greatest extent of melting (>20%), however, lie off of the trend suggested by the other basalt groups and may have re-equilibrated with a lower fO_2 mantle source or a lower crustal composition. In addition to correlations between the addition of the subduction component and oxygen fugacity, as the temperature of melt segregation decreases, the oxidation state of the melt increases (Fig. 31b). The correlation between temperature and oxidation state may result in response to lower peridotite melting temperatures resulting from the addition of an increasing amount of a hydrous subduction component (i.e. Gaetani and Grove, 1998; Stopler and Newman, 1994)

MELT PATHWAYS AND MANTLE OXIDATION STATES

The timing of melt segregation from the mantle relative to partial melting is thought to exert significant control on the variations in basalt oxidation state. Previous studies, summarized by Parkinson and Arculus (1999) suggest that 1) decompression melting may result in an increase of 0.6-0.8 log fO_2 units for every 10kbar of decompression, provided the melts stay in equilibrium with their mantle source (i.e. batch melting; Ballhaus and Frost, 1994) and that 2) for fractional melts, closed to oxygen, magmas do not experience a significant change in fO_2 as a result of decompression (<0.5

log units for 3 Gpa of decompression; Kress and Carmichael, 1991). In either scenario

the basaltic melts appear to record the oxidation state of the mantle that they were last in

equilibrium with although only melts that have been extracted shortly after partial

melting (i.e. fractional melting) appear to maintain the oxidation state of their original

parental mantle. A third scenario is that fractional melting is occurring during

decompression of the mantle followed by aggregation of the melt, in which case the

oxidation state of the magma is dependent on the pressure of melt aggregation (Parkinson

and Arculus, 1999).

In order to relate the measured oxygen fugacities of the basaltic magmas to their

respective mantle sources we must evaluate the significance of the two melt extraction

models on the oxidation state of the basaltic magmas. Pressures of melt segregation for

melt inclusions have been calculated using the Albarede (1992) geobarometer, following

the methodology of Leeman et al (2005) to evaluate the range of pressures over which

melts are being extracted from their mantle source. Melts which have stayed in

equilibrium with their mantle source during decompression melting would likely have a

relatively shallow extraction depth whereas fractional melts would likely be extracted

from significantly greater depths. In the case of the third melting scenario, melt

segregation depths may record the pressure of aggregation (if melts re-equilibrate with

the mantle at aggregation depths) or they may record fractional melting over a wide range

of pressures.

Melt inclusion compositions have been recalculated by adding equilibrium olivine

in 0.4 wt% increments until melt compositions are in equilibrium with Fo_{90} olivine in

order to approximate mantle conditions. A detailed discussion of the problems associated with recalculating melt compositions for use with the Albarede (1992) geobarometer is provided by Leeman et al (2005), however, by utilizing primitive olivine-hosted melt inclusions for this procedure much of the uncertainty associated with late fractional crystallization is avoided.

Application of the Albarede (1992) geobarometer for calculation of depths of melt segregation in this study is dubious because of the large uncertainties in recalculation of the parental melt compositions and in the subarc mantle thermal structure (i.e. what would the effect of an inverted thermal gradient be on the calculated pressures?), and lack of calibration of the geobarometer for the presence of volatile phases (Albarede, 1992, Leeman et al., 2005). However, for a given sample, the variations in calculated pressure should reasonably approximate the range of melt segregation pressures, even if absolute pressures cannot be accurately determined (Fig. 32). In general, two important observations can be made with regard to the segregation pressures of the melt inclusions.

1. OIB-like and shoshonitic melt inclusions generally have a 4.5-2.5 kbar, respectively, greater range in segregation pressures than CAB or LKT inclusions. This may suggest that these melts are less likely to have re-equilibrated during aggregation at shallower pressures. Shoshonitic melt inclusions are not depicted in Figure 32 because of the great uncertainties in estimating pressures for melts with very high water contents. However, while the absolute pressures are likely not valid the range of pressures is believed to be relatively representative.
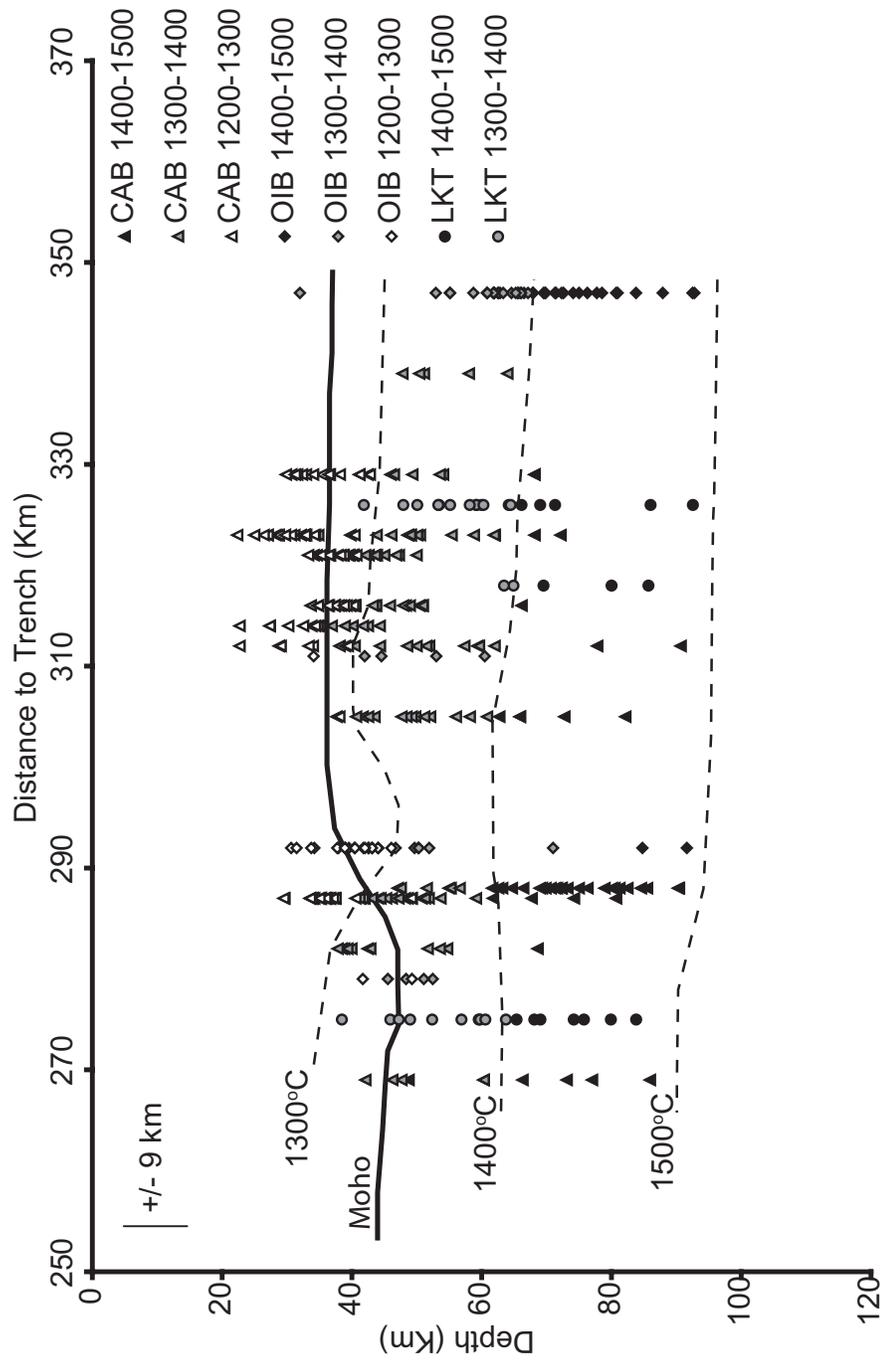
Figure 32. Calculated depths and temperatures of melt inclusion segregation from a mantle source after Leeman et al (2005). Estimated error on depth calculation is +/- ~9 km (Albarede, 1992) however depths should be considered on a relative basis only (see text). Dashed lines are isotherms based on Sugawara (2000) geothermometer. Shoshonitic basalts are not plotted due to the large uncertainty in calculated pressures as a result of high water contents. Seismic moho from Catchings and Mooney (1988) and Stanley et al (1990).

2. Despite similar ranges in calculated pressures low-K tholeiitic inclusions have a greater average pressure of segregation than CAB pressures which typically have segregation pressures equivalent to the base of the crust (~45 km; Stanley et al., 1990; Catchings and Mooney, 1988). The low pressure of melt segregation may indicate that CAB melts are 1) derived from a shallower mantle source (enriched lithospheric mantle), that 2) the melts are aggregating and re-equilibrating at the base of the crust or 3) CAB melts are remaining in equilibrium with the mantle source during decompression (Fig. 32).

Based on the observation that CAB inclusions deviate significantly from the correlation between SC added to the mantle source and oxidation state observed in other basalt groups in conjuction with the low pressures of melt segregation it may be argued that only the CAB inclusions are not representative of their initial peridotite source. Based on the estimates of SC addition, CAB inclusions are anticipated to have an oxidation state of +1 to +1.5 log units (ΔFMQ) rather than the measured -0.25 log units (ΔFMQ) to FMQ (Fig. 31a). The lower than expected oxidation states of CAB inclusions may suggest that equilibrium decompression melting is not occurring, as this melting process is predicted to result in an increase in basaltic fO_2 rather than a reduction (Parkinson and Arculus, 1999; Ballhaus and Frost, 1994). CAB magmas therefore, are likely aggregating and re-equilibrating with a more reduced composition resulting in significantly lower than predicted oxidation states. Despite complications associated with the CAB melt inclusions, differences in basalt fO_2 from OIB-like, LKT and

shoshonitic melt inclusions appear to be representative of relative differences in their respective mantle sources, likely a function of the addition of a subduction component from the subducting Juan de Fuca plate.

SUMMARY OF CONCLUSIONS

Several important conclusions may be drawn from the examination of trace element and volatile element variation, and oxidation state with regard to the addition of a subduction component to the subarc mantle beneath the Oregon Cascades.

1. OIB-like and shoshonitic basalts have the greatest across arc geochemical variations while LKT and CAB melt inclusions are relatively similar between the arc and backarc (Fig. 21, 23).

2. Correlation of fluid mobile elements and volatiles with sulfur speciation and fO_2 suggests that the addition of a subduction component added to the subarc mantle resulted in the generation of more highly oxidized, fluid-mobile element rich basaltic compositions nearer to the trench (Fig. 29).

3. Flux melt modeling of basaltic melt inclusions generally indicates an increase in wt% subduction component added to the mantle source region from backarc to forearc within individual basalt groups, excluding CAB melt inclusions (Fig. 30).

4. The absence of a significant across-arc variation in CAB melt compositions may indicate that CAB trace element signatures present in the backarc are the result of a prior enrichment event and not related to current subduction (Fig. 21). High degree

melting, shallow mantle segregation depths and low measured fO$_2$ may indicate that CAB melts re-equilibrated with a more reduced composition prior to eruption and are therefore not representative of their initial mantle oxidation states predicted as a result of the addition of a subduction component (Fig. 30, 32).

5. The overall range in basaltic fO$_2$ is from less than -0.25 log units to +1.9 log units (> 2.25 log units) relative to the FMQ oxygen buffer and that this range is believed to be representative of the overall variation in mantle source oxidation states (Fig. 28).

ACKNOWLEDGEMENTS

REFERENCES

Albarede, F. (1992). How deep do common basaltic magmas form and differentiate? Journal of Geophysical Research, 97, 10997-11009.

Anderson, A.T., and Wright, T.L. (1972). Phenocrysts and glass inclusions and their bearing on oxidation and mixing of basaltic magmas, Kilauea Volcano, Hawaii. American Mineralogist, 57, 188-216.

Arculus, R.J. (1985). Oxidation status of the mantle: past and present. Annual Review of Earth and Planetary Sciences, 13, 75-95.

Bacon, C. (1990). Calc-alkaline, shoshonitic, and primitive tholeiitic lavas from monogenetic volcanoes near Crater Lake, Oregon. Journal of Petrology, 31, 135-166.

Bacon, C., Bruggman, P., Christiansen, R., Clynne, M., Donnelly-Nolan, J., and Hildreth, W. (1997). Primitive magmas at five Cascade volcanic fields: melts from hot, heterogeneous sub-arc mantle. The Canadian Mineralogist, 35, 297-423.

Baker, M.B. Grove, T.L., and Price, R. (1994). Primitive basalts and andesites from the Mt. Shasta region, N. California: products of varying melt fraction and water content. Contributions to Mineralogy and Petrology, 118, 111-129.

Ballhaus, C. (1993). Redox states of lithospheric and asthenospheric upper mantle. Contributions to Mineralogy and Petrology, 114, 331-348.

Ballhaus, C., and Frost, B.R. (1994). The generation of oxidized CO_2-beraing basaltic melts from reduced CH_4-bearing upper mantle sources. Geochimica et Cosmochimica Acta, 58, 4931-4940.

Ballhaus, C., Berry, R.F., and Green, D.H. (1991). High pressure experimental calibration of the olivine-orthopyroxene-spinel oxygen geobarometer: implications for the oxidation state of the upper mantle. Contributions to Mineralogy and Petrology, 107, 27-40.

Ballhaus, C., Berry, R.F., and Green, D.H. (1990). Oxygen fugacity controls in the Earth's upper mantle. Nature, 348, 437-440.

Barnes, S.J. (1998). Chromites in komatiites, 1. magmatic controls on crystallization and composition. Journal of Petrology, 39, 1689-1720.

Beyer, R. (1973). Magma differentiation at Newberry Crater in central Oregon. Ph.D. Thesis, University of Oregon, Eugene, Oregon, 93.

Bezos, A., and Humler, E. (2005). The Fe3+/ΣFe ratios of MORB glasses and their implications for mantle melting. Geochimica et Cosmochimica Acta, 69, 711-725.

Borg, L.E., Blichert-toft, J., and Clynne, M.A. (2002). Ancient and modern subduction zone contributions to the mantle sources of lavas from the Lassen region of California inferred from Lu-Hf isotopic systematics. Journal of Petrology, 43, 705-723.

Borg, L.E., Clynne, M.A., and Bullen, T.D. (1997). The variable role of slab-derived fluids in the generation of a suite of primitive calc-alkaline lavas from the southernmost Cascades, California. The Canadian Mineralogist, 35, 425-452.

Bostock, M., Hyndman, R., Rondenay, S., and Peacock, S. (2002). An inverted continental Moho and serpentinization of the forearc mantle, Nature, 417, 536-538.

Brandon, A.D., and Draper, D.S. (1996). Constraints on the origin of the oxidation state of mantle overlying subduction zones: an example from Simcoe Washington, USA. Geochimica et Cosmochimica Acta, 60, 1739-1749.

Carmichael, I.S.E., and Ghiorso, M.S. (1986). Oxidation-reduction relations in basic magma: a case for homogenous equilibria. Earth and Planetary Science Letters, 78, 200-210.

Carmichael, I.S.E., and Ghiorso, M.S. (1990). The effect of oxygen fugacity on the redox state of natural liquids and their crystallizing phases. In: Modern Methods of Igneous Petrology: Understanding Magmatic Processes, J. Nicholls and J.K. Russel (eds). Reviews in Mineralogy, 24, 191-212.

Carroll, M., and Rutherford, M. (1988). Sulfur speciation in hydrous experimental glasses of varying oxidation state: Results from measured wavelength shifts of sulfur X-rays. American Mineralogist, 73, 845-849.

Carroll, M.R., and Webster, J.D. (1994). Solubilities of sulfur, noble gases, nitrogen, chlorine, and fluorine in magmas. In Volatiles in Magmas, M.R. Carroll and J.R. Holloway (eds). Reviews in Mineralogy, 30, 231-279.

Catchings, R.D., and Mooney, W.E. (1988). Crustal structure of east central Oregon: relation between Newberry volcano and regional crustal structure. Journal of Geophysical Research, 93, 10081-10094.

Churikova, T., Dorendorf, F., and Worner, G. (2001). Sources and fluids in the mantle wedge below Kamchatka, evidence from across-arc geochemical variation. Journal of Petrology, 42, 1567-1593.

Christie, D.M., Carmichael I.S.E., and Langmuir, C.H. (1986). Oxidation states of mid-ocean ridge basalt glasses. Earth and Planetary Science Letters, 79, 397-411.

Clynne, M.A., and Borg, L.E. (1997). Olivine and chromian spinel in primitive calc-alkaline and thoeiitic lavas from the southernmost Cascade range, California: a reflection of relative fertility of the source. The Canadian Mineralogist, 35, 453-472.

Conrey, R., Sherrod, D., Hooper, P., and Swanson, D. (1997). Diverse primitive magmas in the Cascade arc, Northern Oregon and Southern Washington: The Canadian Mineralogist, 35, 367-396.

Conrey, R.M., Taylor, E.M., Donnelly-Nolan, J.J., Sherrod, D. (2002). North-Central Oregon Cascades: exploring petrologic and tectonic intimacy in a propagating intra-arc rift. In: Field Guide to Geologic Processes in Cascadia (ed. G. Moore). Oregon Department of Geology and Mineral Industries Special Paper 36, 47-90.

Danyushevsky, L. V., Della-Pasqua, F.N., and Sokolov, S. (2000). Re-equilibration of melt inclusions trapped by magnesian olivine phenocrysts from subduction-related magmas: petrological implications. Contributions to Mineralogy and Petrology, 138, 68-83.

Danyushevsky, L. V., McNeill, A.W., and Sobolev, A. (2002). Experimental and petrological studies of melt inclusions in phenocrysts from mantle-derived magmas: an overview of techniques, advantages and complications. Chemical Geology, 183, 5-24.

Davies, J.H., and Stevenson, D.J. (1992). Physical model of source region of subduction zone volcanics. Journal of Geophysical Research, 97, 2037-2070.

Duncan, R.A., Hooper, P.R., Rehacek, J., Marsh, J.S. and Duncan, A.R. (1997). The timing and duration of the Karoo igneous event, southern Gondwana. Journal of Geophysical Research, 102, 18127-18138.

Duncan, R.A. and Keller, R.A. (2004). Radiometric ages for basement rocks from the Emperor Seamounts, ODP Leg 197. Geochemistry, Geophysics, Geosystems, doi: 10.1029/2004GC000704.

Gaetani, G.A., and Grove, T.L. (1998). The influence of water on melting of mantle peridotite. Contributions to Mineralogy and Petrology, 131, 8309-8318.

Ghiorso, M.S., and Carmichael, I.S.E. (1987). Modeling magmatic systems: petrologic applications. In Thermodynamic modeling of geological minerals, fluids and melts, I.S.E. Carmichael and H.P. Eugster (eds.), Reviews in Mineralogy, 17, 467-499.

Grove, T.L., Parman, S.W., Bowring, S.A., Price, R.C., and Baker, M.B. (2003). The role of an H_2O-rich fluid component in the generation of primitive basaltic andesites and andesites from the Mt. Shasta region, N. California. Contributions to Mineralogy and Petrology, 142, 375-396.

Guffanti, M., and Weaver, C. (1988). Distribution of late Cenozoic volcanic vents in the Cascade range: volcanic arc segmentation and regional tectonic considerations: Journal of Geophysical Research, 93, 6513-6529.

Harris, R., Iyer, H., and Dawson, P. (1991). Imaging the Juan de Fuca plate beneath southern Oregon using teleseismic P-wave residuals. Journal of Geophysical Research, 96, 19879-19889.

Harry, D.L., and Green N.L. (1999). Slab dehydration and basalt petrogenesis in subduction systems involving very young oceanic lithosphere. Chemical Geology, 160, 309-333.

Hauri, E. H. (2002). SIMS analysis of volatiles in silicate glasses, 2: isotopes and abundances in Hawaiian melt inclusions. Chemical Geology, 183, 115-141.

Higgins, M. (1973). Petrology of Newberry Volcano, Central Oregon. Geological Society of America Bulletin, 84, 455-487.

Hochstaedter, A.G., Gill, J.B., Taylro, B., Ishizuka, O., Yuasa, M., and Morita, S. (2000). Across-arc geochemical trends in the Izu-Bonin arc: constraints on source composition and mantle melting. Journal of Geophysical Research, 105, 495-512.

Hochstaedter, A., Gill, J., Peters, R., P, B., Holden, P., and Taylor, B. (2001). Across-arc geochemical trends in the Izu Bonin arc: Contributions from the subducting slab: G-cubed, 2, 2000GC000105.

Jensen, R.A. (2000). Roadside guide to the geology of Newberry Volcano. CenOreGeoPub, Bend, Oregon, 168.

Johnson, D.M., Hooper, P.R., and Conrey, R.M. (1999). XRF analysis of rocks and minerals for major and trace elements on a single low dilution Li-tetraborate fused bead. Advances in X-ray Analysis, 41, 843-867.

Jordan, B.T. (2005). Age-progressive volcanism of the Oregon High Lava Plains; overview and evaluation of tectonic models. In: G.R. Foulger, J.H. Natland, D.C. Presnal, and D.L. Anderson (eds.). Plates, Plumes and Paradigms. Geological Society of America Special Paper, 388, 503-515.

Jordan, B.T. (2001). Basaltic volcanism and tectonics of the High Lava Plains, southeastern Oregon. Ph.D. Thesis, Oregon State University, Corvallis, Oregon, 218.

Jugo, P.J., Luth, R.W., and Richards, J.P. (2005). Experimental data on the speciation of sulfur as a function of oxygen fugacity in basaltic melts. Geochimica et Cosmochimica Acta, 69, 497-503.

Kamenetsky, V.S., Crawford, A.J. and Meffre, S. (2001). Factors controlling chemistry of magmatic spinel: an empirical study of associated olivine, Cr-spinel and melt inclusions from primitive rocks. Journal of Petrology, 42, 655-671.

Kent, A.J.R., Stolper, E.M., Francis, D., Woodhead, J., Frei, R., and Eiler, J. (2004). Mantle heterogeneity during the formation of the North Atlantic Igneous Province: constraints from trace element and Sr-Nd-Os-O isotope sytematics of Baffin Island picrites. Geochemistry, Geophysics, Geosystems, 5, doi: 10.1029/2004GC000743.

Kinzler, R.J., Donnelly-Nolan, J.M., and Grove, T.L. (2000). Late Holocene hydrous mafic magmatism at the Pain Pot crater and Callahan flows, Medicine lake Volcano, N. California and the influence of H2O in the generation of silicic magmas. Contributions to Mineralogy and Petrology, 138, 1-16.

Knaack, C., Cornelius, S.B., and Hooper, P.R. (1994). Trace element analyses of rocks and minerals by ICP-MS. Technical Notes, GeoAnalytical Lab, Washington State University.

Kress, C.V., and Carmichael, I.S.E. (1991). The compressibility of silicate liquids containing Fe_2O_3 and the effect of composition, temperature, oxygen fugacity and pressure on their redox states. Contributions to Mineralogy and Petrology, 108, 82-92.

Leeman, W.P., Lewis, J.F., Evarts, R.C., Conrey, R.M. and Streck, M.J. (2005). Petrologic constraints on the thermal structure of the Cascades arc. Journal of Volcanology and Geothermal Research, 140, 67-105.

Li, Z-X.A., and Lee, C-T, A. (2004). The constancy of upper mantle fO_2 through time inferred from V/Sc ratios in basalts. Earth and Planetary Science Letters, 228, 483-493.

Linneman, S.R. (1990). The petrologic evolution of the Holocene magmatic system of Newberry Volcano, central Oregon. Ph.D. Thesis, University of Wyoming, Laramie, Wyoming, 312.

MacLeod, N., and Sherrod, D. (1988). Geologic evidence for a magma chamber beneath Newberry Volcano, Oregon. Journal of Geophysical Research, 93, 10067-10079.

MacLeod, N., Sherrod, D., Chitwood, L., and Jensen, B. (1995). Geologic map of Newberry Volcano, Deschutes, Kalamath, and Lake Counties, Oregon. U.S. Geological Survey Miscellaneous Map Investigations series Map I-2455.

Mathez, E.A. (1984). Influence of degassing on oxidation states of basaltic magmas. Nature, 310, 371-375.

McCaffrey, R., Long M.D., Goldfinger, C., Zwick, P.C., Nabelek, J.L., Johnson, C.K., and Smith, C. (2000). Rotation and plate locking at the southern Cascadia subduction zone. Geophysical Research Letters, 27, 3117-3120.

McDonough, W.F., and Sun, S.S. (1995). The composition of the Earth. Chemical Geology, 120, 223-253.

Metrich, N., Bonnin-Mosbah, M., Susini, J., Menez, B., and Galoisy, L. (2002). Presence of sulfite (S^{IV}) in arc magmas: Implications for volcanic sulfur emissions. Geophysical Research Letters, 29, 10.1029/2001GL014607.

Metrich, N., Berry, A., O'Neill, H., and Susini, J., 2005, A XANES study of sulfur speciation in synthetic glasses and melt inclusions (abs): Geochimica et Cosmochimica Acta, 69 (10), supplement 1, A51.

Nielsen, R.L., P. Michael, and Sours-Page, R. (1998). Chemical and physical indicators of compromised melt inclusions. Geochimica et Cosmochimica Acta, 62, 831-839.

Ozawa, K. (1984). Olivine-spinel geospeedometry: Analysis of diffusion-controlled Mg-Fe^{2+} exchange. Geochimica et Cosmochimica Acta, 48, 2597-2611.

Parkinson, I.J., and Arculus. R.J. (1999). The redox state of subduction zones: insights from arc peridotites. Chemical Geology, 160, 409-423.

Plank, T., and Langmuir, C.H. (1993). Tracing trace elements from sediment input to volcanic output at subduction zones. Nature, 362, 739-743.

Qin, Z., Lu, F., and Anderson, A.T. (1992). Diffusive reequilibration of melt and fluid inclusions. American Mineralogist, 77, 565-576.

Rasmussen, J., and Humphreys, E. (1988). Tomographic image of the Juan de Fuca Plate beneath Washington and western Oregon using teleseismic P-wave travel times, Geophysical Research Letters, 15, 1417-1420.

Reiners, P.W., Hammond, P.E., McKenna, J.M, and Duncan, R.A. (2000). Young basalts of the central Washington Cascades, flux melting of the mantle and trace element

signatures of primary arc magmas. Contributions to Mineralogy and Petrology, 138, 249-264.

Riddihough, R. (1984). Recent movements of the Juan de Fuca plate system. Journal of Geophysical Research, 89, 6980-6994.

Roedder, E., and Emslie, R. (1970). Olivine-liquid equilibrium. Contributions to Mineralogy and Petrology, 29, 275-289.

Romanyuk, T., Blakely, R., and Mooney, W. (1998). The Cascadia Subduction Zone: two contrasting models of lithospheric structure, Physical Chemistry of the Earth, 23, 297-301.

Romanyuk, T., Mooney, W., and Blakely, R. (2001). Cascade subduction zone, North America: A tectono-geophysical model, Geotectonics, 35, 224-244.

Rowe, M.C., Nielsen, R.L., and Kent, A.J.R. (2006). Anomalously high Fe contents in rehomogenized olivine hosted melt inclusions from oxidized magmas. American Mineralogist, 91, 82-91.

Rowe, M.C., Nielsen, R.L., Kent, A.J., Wallace, P.J., and Donnelly-Nolan, J.M. (2003). Origins of Newberry Volcano: Central Oregon: A Cascade backarc, High Lava Plain, Basin and Range, shield volcano? Eos Trans. AGU, 84 (46), Fall Meet. Suppl., Abstract V32H-06.

Sack, R., Carmichael, I., Rivers, M., and Ghiroso, M. (1980). Ferric-ferrous equilibria in natural silicate liquids at 1 bar. Contributions to Mineralogy and Petrology, 75, 369-376.

Sato, M., and Wright, T.L. (1966). Oxygen fugacities directly measured in magmatic gases. Science 153, 1103-1105.

Schmidt, M.W., and Poli, S. (1998). Experimentally based water budgets for dehydrating slabs and consequences for arc magma generation. Earth and Planetary Science Letters, 163, 361-379.

Scowen, P.A.H., Roeder, P.L., and Helz, R.T. (1991). Reequilibration of chromite within Kilauea Iki lava lake, Hawaii. Contributions to Mineralogy and Petrology, 107, 8-20.

Sherrod, D.R., Taylor, E.M., Ferns, M.L., Scott, W.E., Conrey, R.M., and Smith, G.A. (2004). Geologic map of the Bend 30- x 60-minute quadrangle, Central Oregon. U.S. Geological Survey Geologic Investigations Series Map I-2683.

Sherrod, D.R., and Smith, J.G. (1990). Quaternary extrusion rates of the Cascade range, northwestern United States and southern British Columbia. Journal of Geophysical Research, 95, 19465-19474.

Sobolev, A. V. and Chaussidon, M. (1996). H_2O concentrations in primary melts from suprasubduction zones and mid-ocean ridges: Implications for H_2O storage and recycling in the mantle. Earth and Planetary Science Letters, 137, 45-55.

Stanley, W.D., Mooney, W.D., and Fuis, G.S. (1990). Deep Crustal Structure of the Cascade range and surrounding regions from seismic refraction and magnetotelluric data. Journal of Geophysical Research, 95, 19419-19438.

Stein, S., and Stein, C. (1996) Thermo-mechanical evolution of oceanic lithosphere: implications for the subduction process and deep earthquakes. In: G. Bebout, D. School, S. Kirby, and J. Platt (Eds.). Subduction Top to Bottom. American Geophysical Union Monograph 96, 1-18.

Stern, R.J. (2002). Subduction zones. Reviews of Geophysics, 40, 1012, doi:10.1029/2001RG000108.

Stolper, E., and Newman, S. (1994). The role of water in the petrogenesis of Mariana trough magmas. Earth and Planetary Science Letters, 121, 293-325.

Sugawara, T. (2000). Empirical relationships between temperature, pressure, and MgO content in olivine and pyroxene saturated liquid. Journal of Geophysical Research, 105, 8457-8472.

Tatsumi, Y., Hamilton, D.L., and Nesbitt, R.W. (1986). Chemical characteristics of fluid phase released from a subducted lithosphere and origin of arc magmas: evidence from high-pressure experiments and natural rocks. Journal of Volcanology and Geothermal Research, 29, 293-309.

Trehu, A.M., Asudeh, I., Brocher, T.M., Luetgert, J.H., Mooney, W.D., Nabelek, J.L., and Nakamura, Y. (1994). Crustal architecture of the Cascadia forearc. Science, 266, 237-243.

Verplanck, E.P., and Duncan, R.A. (1987). Temporal variations in plate convergence and eruption rates in the western Cascades, Oregon. Tectonics, 6, 197-209.

Walker, J.A., Roggensack, K., Patino, L.C., Cameron, B.I. and Matias, O. (2003). The water and trace element contents of melt inclusions across an active subduction zone. Contributions to Mineralogy and Petrology, 146, 62-77.